AIP | Physics of Plasmas

The high-foot implosion campaign on the National Ignition Facilitya)

O. A. Hurricane, D. A. Callahan, D. T. Casey, E. L. Dewald, T. R. Dittrich, T. Döppner, M. A. Barrios Garcia, D. E. Hinkel, L. F. Berzak Hopkins, P. Kervin, J. L. Kline, S. Le Pape, T. Ma, A. G. MacPhee, J. L. Milovich, J. Moody, A. E. Pak, P. K. Patel, H.-S. Park, B. A. Remington, H. F. Robey, J. D. Salmonson, P. T. Springer, R. Tommasini, L. R. Benedetti, J. A. Caggiano, P. Celliers, C. Cerjan, R. Dylla-Spears, D. Edgell, M. J. Edwards, D. Fittinghoff, G. P. Grim, N. Guler, N. Izumi, J. A. Frenje, M. Gatu Johnson, S. Haan, R. Hatarik, H. Herrmann, S. Khan, J. Knauer, B. J. Kozioziemski, A. L. Kritcher, G. Kyrala, S. A. Maclaren, F. E. Merrill, P. Michel, J. Ralph, J. S. Ross, J. R. Rygg, M. B. Schneider, B. K. Spears, K. Widmann, and C. B. Yeamans

Citation: Physics of Plasmas (1994-present) **21**, 056314 (2014); doi: 10.1063/1.4874330
View online: http://dx.doi.org/10.1063/1.4874330
View Table of Contents: http://scitation.aip.org/content/aip/journal/pop/21/5?ver=pdfcov
Published by the AIP Publishing

The high-foot implosion campaign on the National Ignition Facility[a)]

O. A. Hurricane,[1,b),c)] D. A. Callahan,[1] D. T. Casey,[1] E. L. Dewald,[1] T. R. Dittrich,[1] T. Döppner,[1] M. A. Barrios Garcia,[1] D. E. Hinkel,[1] L. F. Berzak Hopkins,[1] P. Kervin,[1] J. L. Kline,[2] S. Le Pape,[1] T. Ma,[1] A. G. MacPhee,[1] J. L. Milovich,[1] J. Moody,[1] A. E. Pak,[1] P. K. Patel,[1] H.-S. Park,[1] B. A. Remington,[1] H. F. Robey,[1] J. D. Salmonson,[1] P. T. Springer,[1] R. Tommasini,[1] L. R. Benedetti,[1] J. A. Caggiano,[1] P. Celliers,[1] C. Cerjan,[1] R. Dylla-Spears,[1] D. Edgell,[3] M. J. Edwards,[1] D. Fittinghoff,[1] G. P. Grim,[2] N. Guler,[2] N. Izumi,[1] J. A. Frenje,[4] M. Gatu Johnson,[4] S. Haan,[1] R. Hatarik,[1] H. Herrmann,[2] S. Khan,[1] J. Knauer,[3] B. J. Kozioziemski,[1] A. L. Kritcher,[1] G. Kyrala,[2] S. A. Maclaren,[1] F. E. Merrill,[2] P. Michel,[1] J. Ralph,[1] J. S. Ross,[1] J. R. Rygg,[1] M. B. Schneider,[1] B. K. Spears,[1] K. Widmann,[1] and C. B. Yeamans[1]

[1]*Lawrence Livermore National Laboratory, Livermore, California 94551, USA*
[2]*Los Alamos National Laboratory, Los Alamos, New Mexico 87545, USA*
[3]*Laboratory for Laser Energetics, University of Rochester, Rochester, New York 14623, USA*
[4]*Massachusettes Institute of Technology, Cambridge, Massachusettes 02139, USA*

(Received 31 December 2013; accepted 17 February 2014; published online 22 May 2014)

The "High-Foot" platform manipulates the laser pulse-shape coming from the National Ignition Facility laser to create an indirect drive 3-shock implosion that is significantly more robust against instability growth involving the ablator and also modestly reduces implosion convergence ratio. This strategy gives up on theoretical high-gain in an inertial confinement fusion implosion in order to obtain better control of the implosion and bring experimental performance in-line with calculated performance, yet keeps the absolute capsule performance relatively high. In this paper, we will cover the various experimental and theoretical motivations for the high-foot drive as well as cover the experimental results that have come out of the high-foot experimental campaign. At the time of this writing, the high-foot implosion has demonstrated record total deuterium-tritium yields (9.3×10^{15}) with low levels of inferred mix, excellent agreement with implosion simulations, fuel energy gains exceeding unity, and evidence for the "bootstrapping" associated with alpha-particle self-heating. © *2014 AIP Publishing LLC*. [http://dx.doi.org/10.1063/1.4874330]

I. INTRODUCTION

The energy required to "ignite" fusion fuel scales as the inverse square of the stagnation pressure, $E_{ignition} \sim P_{stag}^{-2}$. For this reason, a key focus of inertial confinement fusion (ICF) research involves achieving stagnation pressures in excess of 300 Gbars. A carefully orchestrated cascade of energy from larger spatial scales to smaller, through a convergent implosion, is how such large pressures are generated. On the National Ignition Facility (NIF),[1] 192 laser beam lines deliver up to 1.8 MJ of 0.35 μm wavelength UV light into a cylindrical gold hohlraum that converts $\sim 2/3$ of the energy into a nearly Planckian bath of x-rays. The x-rays are absorbed by a $\sim$1 mm radius capsule with an energy efficiency of $\sim 10\% - 20\%$ generating $\sim$100 Mbars pressure in the ablator—the 195 μm (in this case) thick outer shell of the capsule. This ablation pressure, delivered as a series of shocks, accelerates the capsule inwards to speeds of $\sim 300 - 400$ km/s. Coated on the inside of the ablator is the deuterium-tritium (DT) fusion fuel layer, which is initially in a cryogenic ice state of $\sim$70 μm thickness. Ideally, by the time the implosion achieves its peak velocity, the DT fuel has become a Fermi degenerate gas with $\sim 10 - 14$ kJ of kinetic energy. As the fuel stagnates at the center of the implosion, kinetic energy is converted into work (pdV) and internal energy as the DT fuel forms a hot-spot from the fuel's inner surface. The hot-spot initiates the fusion reactions, producing neutrons and alpha-particles as the hot-spot ion temperature climbs to many keV. At sufficiently high hot-spot areal density, $(\rho r)_{hs} > 0.3$ g/cm^2 and ion temperature, $T_{ion} > 4$ keV, the hot-spot will "ignite" as alpha-particles redeposit their energy locally creating self-heating and, if $(\rho r)_{fuel} > 1$, heating will propagate from the hot-spot into the cold fuel releasing energy many times greater than that absorbed by the capsule. Creating the required conditions for ignition in the laboratory has been challenging[2] and has yet to be achieved at any fusion research facility.

The U.S. National Ignition Campaign (NIC)[3] collaboration on the NIF was a joint effort between Lawrence Livermore, Los Alamos, Sandia National Laboratories, General Atomics (GA), the Laboratory for Laser Energetics (LLE), and the MIT Plasma Science and Fusion Center, with contributions from the Naval Research Laboratory, the Commissariat à l'énergie atomique (CEA), and the Atomic Weapons Establishment (AWE). The NIC had two primary purposes, to attempt to demonstrate ignition before the end of 2012 and to demonstrate a wide array of diagnostics, experimental platforms, and analysis techniques that would be needed for future high-energy density physics and ICF research. These platforms, diagnostics, and analysis techniques were used during the high-foot implosion campaign.

[a)]Paper QI3 4, Bull. Am. Phys. Soc. **58**, 279 (2013).
[b)]Invited speaker.
[c)]Electronic address: hurricane1@llnl.gov

II. HIGH-FOOT PULSE-SHAPE

Near the end of 2012, an international workshop was convened to address the physics difficulties that were apparent in the NIC. A number of strategies were suggested in order to address the physics that was frustrating the NIC implosion.[4] The high-foot implosion[5–7] was developed primarily to test the hypothesis that ablation-front Rayleigh-Taylor (A-RT) instability[8] was responsible for a significant fraction of the degraded implosion performance observed during the NIC.[2,9] The high-foot also appeared, in simulations, to ameliorate a sensitivity of the ablation front-profile to opacity modeling.[5] The high-foot campaign began using the same target geometry and material (CH plastic capsules) as the NIC Rev. 5 design[10]—a practical choice dictated by logistics of obtaining targets when the effort began—but the laser pulse-shape is different (see Fig. 1, left frame).

In order to create a higher hohlraum radiation temperature, T_r, in the early-time "foot" of the drive (hence "high-foot"), the initial picket of the laser pulse is approximately doubled as compared to the low-foot drive, thus launching a stronger and faster first shock (the shock speed scales as $u_s \sim T_r^{1.75}$) into the ablator of the capsule. The laser power in the trough (the time between the first and second shocks) is also higher than the low-foot in order to maintain an approximately constant $T_r \sim 90$ eV in the foot. A consequence of the higher T_r at early time is a more rapid ablation of the capsule (the ablation velocity scales as, $v_a \sim T_r^{9/10}$, Ref. 19). The stronger/faster first shock places both the ablator and the DT ice on a higher adiabat, α, than that of the low-foot pulse shape. In terms of the definition of DT adiabat that is a ratio between the DT pressure and the minimum DT equation of state (EOS) pressure at 1000 g/cc,[10] $\alpha = P/P_{cold}$ (note the alternate definition of $\alpha = P/P_{Fermi}$, where P_{Fermi} is the Fermi pressure) the high-foot pulse-shape design used in our campaign has fuel $\alpha \sim 2.5$, whereas the low-foot point design ideally has fuel $\alpha \sim 1.45$.

In order the maintain the correct shock merger depth in the DT ice for the first and subsequent shocks, the time duration of the trough is shortened by approximately 5 ns as compared to the low-foot pulse. Additional features of the high-foot pulse-shape are the dropping of one shock (that would correspond to dropping shock number "2" in the four shock low-foot pulse) and a reduction of the peak laser power (for better hot-spot shape control) associated with driving the final shock. Dropping the number of shocks in the high-foot from 4 to 3 was motivated by a desire to reduce potential Richtmyer-Meshkov (RM) instability and vorticity generation at the fuel-ablator interface, but also had the practical benefit of simplifying the complexity of shock timing and reducing the number of "keyhole" experiments needed.[11,12]

Some elements of the high-foot pulse-shape are recognizable in the direct-drive high-adiabat pulse shape of the LLE.[13,14] Namely, the LLE high-adiabat pulse essentially doubles the laser power in the early part of the pulse that launches the first and second shocks as compared to the low-adiabat pulse-shape (see Fig. 1, right frame). Like the high-foot pulse, the high-adiabat pulse is of shorter time duration than the low-adiabat pulse. Unlike the high-foot pulse, the LLE high-adiabat pulse-shape is still a four shock pulse-shape and the peak power was left the same as the low-adiabat pulse. The goals of the LLNL high-foot and LLE high-adiabat pulse shape are essentially the same: create a more stable implosion at the cost of theoretical fuel compression.

III. HIGH-FOOT STABILITY

The essential stability benefits of the high-foot scheme can be understood from examining an expression for the linear growth-rate of ablation driven RT instability[15]

$$\gamma_{A-RTI} = \alpha_2(Fr,\nu)\sqrt{\frac{kg}{1+kL_\rho}} - \beta_2(Fr,\nu)kv_a \qquad (1)$$

where k is the perturbation wavenumber, g is the ablator acceleration, L_ρ is the density gradient scale-length of the ablation front, and α_2 and β_2 are parameters of order unity whose exact values depend upon a heat conduction scale-length parameter, ν, and the Froude number, $Fr = v_a^2/(gL_\rho)$. The key stabilizing effects of the high-foot drive enter through the higher ablation velocity increasing the $\beta_2 kv_a$ ablative stabilization term of Eq. (1) and through an increase in L_ρ which reduces the $\sqrt{kg}$ unstable RT drive term. The increase in L_ρ is primarily due to a stronger 1^{st} shock which

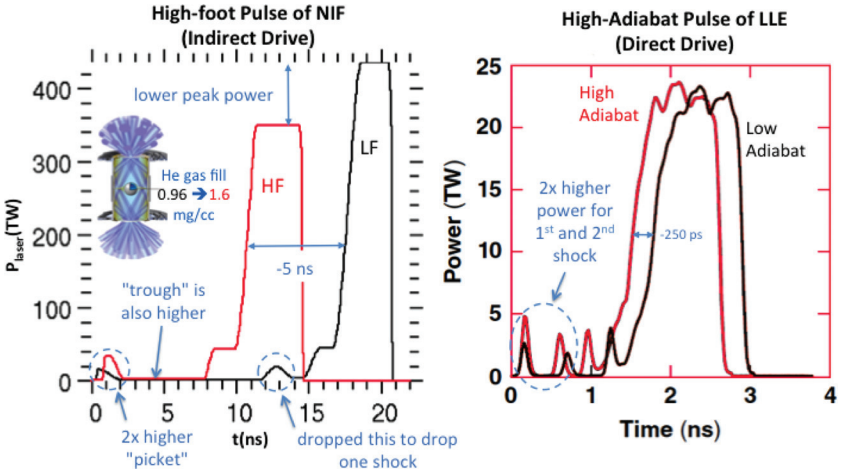

FIG. 1. (Left frame) The NIF indirect drive high-foot pulse-shape (red) is juxtaposed with the low-foot pulse-shape (black) with the salient features identified. (Right frame) The LLE direct drive high-adiabat pulse-shape is shown with the low-adiabat pulse-shape. The high-foot pulse launches three shocks, while the others launch four shocks. Inset: The NIF hohlraum-capsule geometry is shown with laser beams impinging upon the target.

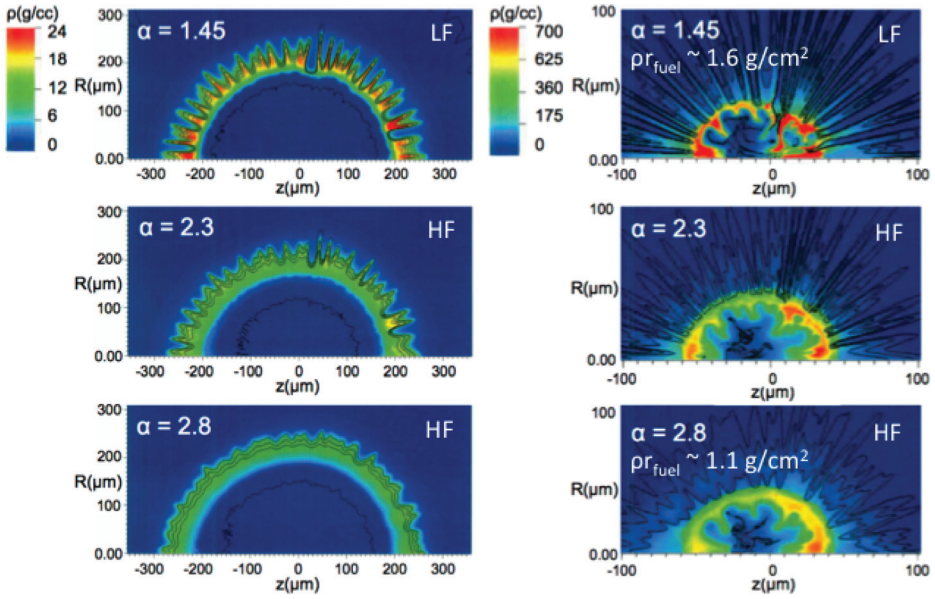

FIG. 2. Capsule-only multimode stability calculations of the low-foot (top row) implosion and two high-foot (second and third rows) implosions are shown. The left column shows the condition of the ablator (on a density color scale) at 200 μm radius which is near peak velocity and the right column shows the condition of the ablator and hot-spot at peak compression. The trade-off between densification and stability are clear. Reprinted with permission from Phys. Rev. Lett. **112**, 055002 (2014). Copyright 2014 AIP Publishing LLC.

increases the adiabat of the implosion and prevents the ablator from becoming so highly compressed (risking break-up) during the implosion.

Two-dimensional (2D) ARES[16,17] multimode (modes <100) simulations using a measured surface roughness spectrum capture the enhanced stability benefits of the high-foot drive (Fig. 2). These simulations, with a multiplier of 4 on the amplitude of the applied surface perturbations (applied to all interfaces including the ice layer, Fig. 2), show how the low-foot ablator could begin to break-up around the time of peak velocity and not be intact at peak compression, therefore disrupting the formation of the hot-spot, whereas higher-foot implosions would be resistant to RT driven ablator breakup. The factor of 4 was chosen because the yield in the 2D low-foot simulation is degraded by a factor of $\sim$10 as compared to 1D simulations of the same implosion, roughly corresponding the observed yield deficit for the low-foot.[18] The higher the foot level, as measured by the adiabat, α, and shown in Fig. 2, the less high-mode instability growth is observed but with a concomitant reduction in fuel compression and stagnation pressure.

The enhanced stability can be further and most simply understood by comparing the in-flight-aspect ratios (IFARs), $R_{in}/\Delta R$, where R_{in} is the ablator inner radius and ΔR is the ablator thickness: for the high-foot implosion, the IFAR is roughly half of that of the low-foot implosion (Fig. 3). The amplitude of instability growth is directly related to the exponent of $\sqrt{R_{in}/\Delta R}/2$ (Ref. 19) but it is also intuitively obvious that a thicker ablator traveling the same total distance would be less susceptible to break-up than a thinner one. The fact that the high-foot ablator is roughly $\sim 2\times$ thicker than the low-foot ablator was confirmed in streaked radiography experiments of the high-foot implosion (shot N130409, inset in Fig. 3 and also see Appendix A).

Framing camera images (backlit absorption) of the high-foot capsule near peak velocity (and radius $R \sim 200$ μm), the primary purpose of which is to obtain ablator shape data,[20,21] gave the first incidental indications of reduced A-RT instability. The low-foot implosion develops rips from A-RT growth along lines of latitude across the circumference of the capsule (Fig. 4, left frame), seeded by the two circles of contact between the capsule and the drumhead-like membranes (the "tent" made of plastic), of 110 nm thickness in this case, which holds the capsule in the center of the hohlraum. High-foot implosions (center frame and right frame of Fig. 4) show no such tent generated perturbation. Later, direct experimental demonstrations of greatly reduced A-RT instability using the high-foot pulse-shape, in the linear regime, were performed using face-on radiography of pre-imposed capsule perturbations.[22,23]

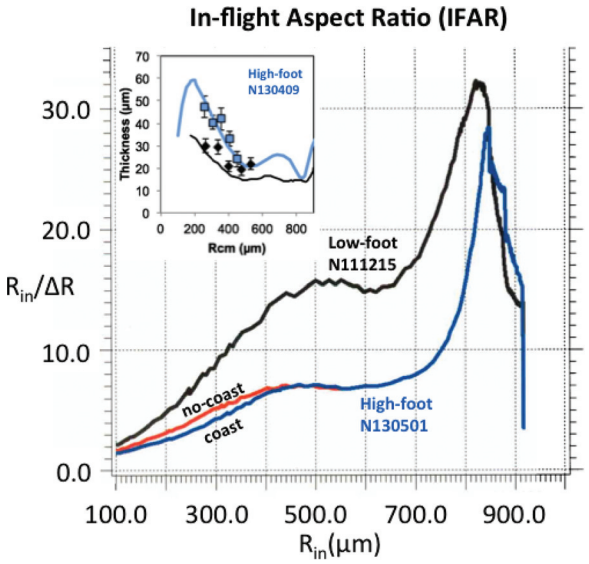

FIG. 3. Simulated inflight-aspect-ratio vs. fuel-ablator interface radius for high-foot (blue and red) and low-foot (black) implosions are plotted. Throughout most of the implosion, the high-foot case has *IFAR* that is half of the low-foot case. Confirmation of the *IFAR* was validated by streaked radiography experiments (N130409) of the implosion that give the ablator thickness as a function of ablator center-of-mass radius (inset). Experimental data are given as points with error bars in the inset and results from simulations are shown as curves.

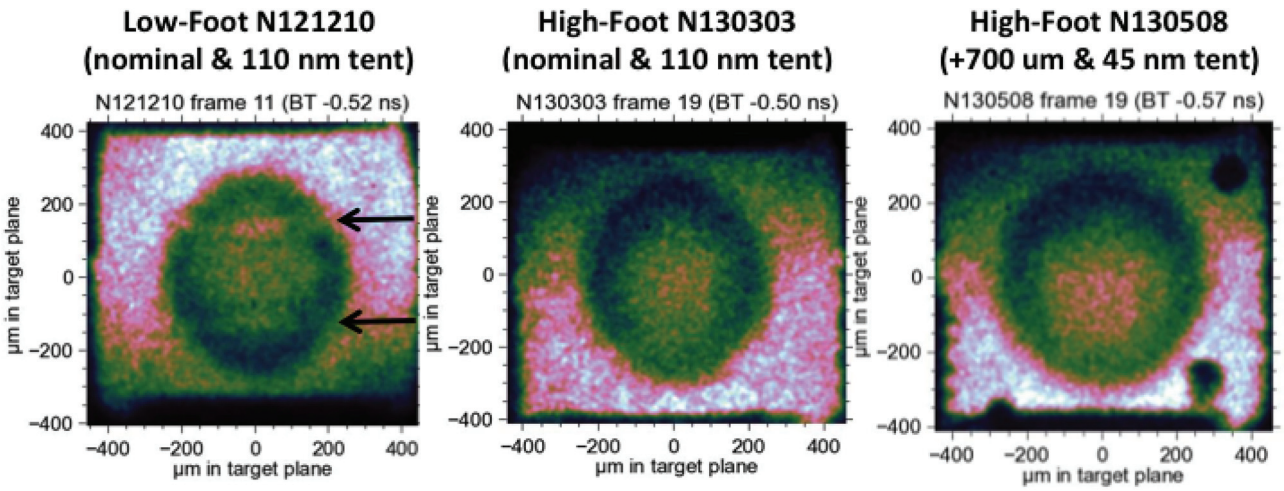

FIG. 4. Backlit x-ray absorption imaging of ablators near peak velocity are shown for a low-foot implosion (left frame) and two high-foot implosions (middle and right frames). The two horizontal bands in the left frame show a perturbation in the ablator that was initiated by the 110 nm plastic membrane ("tent") that holds the capsule in place in its as-built configuration. The middle image shows no evidence of the tent perturbation even though the tent thickness was the same as for the low-foot implosion shown in the left frame. The right frame corresponds to a high-foot implosion in a longer hohlraum, which improves the ablator shape,[20] and also shows no evidence for a tent induced perturbation, the as-built tent being 45 nm thick in this case.

IV. IMPLOSION PERFORMANCE

After a number of preparatory experiments and analysis to establish shock timing, hot-spot shape control, ablator shape, ablator-hohlraum energy coupling, and implosion trajectory (see Appendix A) for the high-foot pulse-shape, a series of cryogenic DT layer implosion experiments established the integrated target performance under various drive conditions (see Table I). Key measured quantities are neutron yield, Y_{13-15}, in the 13-15 MeV energy band around the characteristic 14.1 MeV DT fusion neutron energy, burn averaged ion-temperature (T_{ion}), neutron and x-ray burn-widths (τ_n and τ_x), down-scatter-ratio (*DSR*), and the time of peak neutron brightness ("bang-time"). On the NIF, Y_{13-15} is an average of many diagnostics including four neutron time-of-flight (NToF) detectors,[24] numerous radiochemical activation measurements,[25] and a magnetic recoil spectrometer (MRS).[26] T_{ion} is directly related to the temporal spread

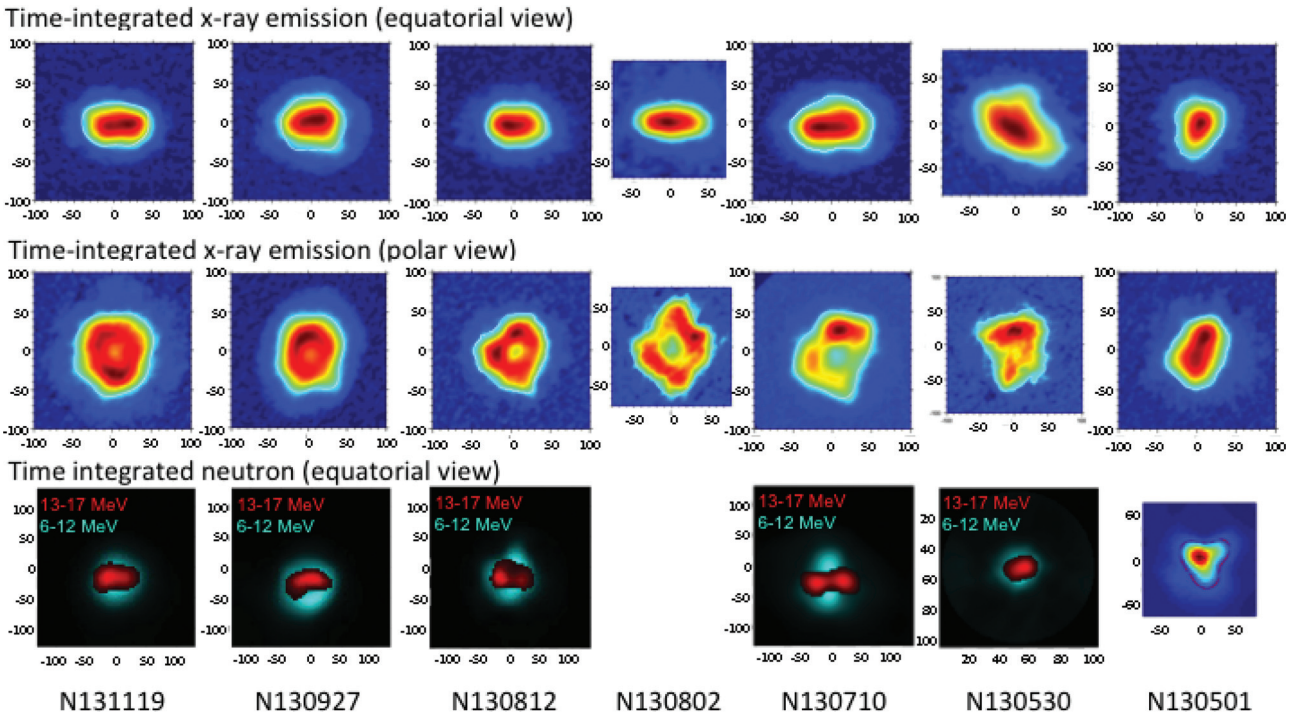

FIG. 5. Shown are the series of high-foot DT layer experiments time-integrated imaging results. The top row shows equatorial x-ray shape, the middle row shows polar x-ray shape, and the bottom row shows neutron imaging (red being direct 13-17 MeV neutrons and cyan being down-scattered 6-12 MeV neutrons). Note for N130501 the observed M2 mode in the polar image is due to windows in the wall of the hohlraum that are aligned with the elongated shape. Also for N130501, only the direct neutron image is shown. N130802 did not produce a useful neutron image due to its low yield. Dimensions are in μm. We note, unsurprisingly, that the two implosions with the most distorted shapes, N130530 and N130802, also had longest burn-widths (see Table I).

obtained from the full-width-half-max (FWHM) of the NToF detectors (for both DT and DD reactions). A temporal gamma ray history gives τ_n. The *DSR* comes from measuring, via NToF and MRS, the number of neutrons scattered into the energy range of 10–12 MeV and is directly related to the areal density of the cold DT fuel, $(\rho r)_{fuel} \approx 20.3 \cdot f \cdot DSR$ (where f depends upon the amount of ablator mass remaining but is typically 0.95 ± 0.05).[26,27] Other diagnostics, such as x-ray imaging[28] (from time-integrated image plates, shown, and time-resolved gated imaging, not shown) and neutron imaging[29–31] (Fig. 5), give information on the shape of the implosion (expressed in Legendre modes for the equatorial view and Fourier modes for the polar view). Coefficients of the Legendre and Fourier expansions describing shape are given as the P's and M's shown in Table I (with the subscript x standing for time-integrated x-ray and the n standing for imaging for direct 13–17 MeV and downscattered 6–12 MeV neutrons).

Shots N130501, N130710, N130812, N130927, and N131119 (NIF shots are named in a year-month-day format, YYMMDD, thus N130501 was shot on May 1, 2013) constitute a logical series over various laser powers and energies using the same "nominal" hohlraum geometry and with capsules ("T0" thickness of $\sim$195 μm) and ice layers that were largely within specified tolerances. The nominal hohlraum is a gold can of 5.75 mm diameter and 9.425 mm length with a laser entrance hole (LEH) of 3.101 mm radius (see inset in Fig. 1). The same hohlraum geometry was used during the NIC for most of the low-foot shots.

As is typical for the high-foot series, the hohlraum is filled with helium gas of 1.6 mg/cc density (as compared to 0.96 mg/cc for the NIC) the purpose of which is to restrict and delay gold plasma for blowing in from the inside wall of the hohlraum which can otherwise impede laser beam propagation. Additionally, by redistributing energy between different laser beams, through laser light wavelength changes that affect the cross-beam-energy-transfer (CBET)[32–35] (the transfer of power from one beam to another via induced Brillouin scattering), the illumination pattern in the hohlraum has been varied over the campaign in order to better optimize the implosion shape. In particular, wavelength differences $\Delta\lambda_{23.5}$, between the 23.5° beams and outer cone beams, and $\Delta\lambda_{30}$, between the 30° beams and outer cone beams, affect equatorial symmetry while $\Delta\lambda_{23.5-30}$, between the 23.5° and 30° beams, affects azimuthal symmetry. Prior to shot N130927, $\Delta\lambda_{23.5-30} = 1.2$Å was used on all shots, while for N130927 and all subsequent shots $\Delta\lambda_{23.5-30} = 0.7$Å was used (the effect on polar shape can be seen in Fig. 5). The $\Delta\lambda$'s for equatorial shape control are listed in Table I.

In Fig. 5 and Table I, it can be observed (shots N130501 and N130710) that upon increasing the laser power (in order to drive up the hohlraum T_r and therefore implosion speed,

TABLE I. High-foot DT shot measurements with T0 capsules.

Quantity	N131119	N130927	N130812	N130802	N130710	N130530	N130501
NIF power (TW)	425	390	355	430	430	430	351
NIF energy (MJ)	1.88	1.82	1.69	1.48	1.47	1.45	1.27
$\Delta\lambda_{23.5}/\Delta\lambda_{30}$ (Å)	9.5/8.8	9.2/8.5	8.5/7.3	9.4/8.4	8.5/7.3	8.5/7.3	8.5/7.3
Backscatter (kJ)	242.76	192.11	245.06	193.83	186.36	197.84	…
Y_{13-15} ($\times 10^{15}$)	5.2 ± 0.097	4.4 ± 0.11	2.4 ± 0.048	0.48 ± 0.012	1.05 ± 0.02	0.58 ± 0.012	0.77 ± 0.016
T_{ion} (keV) DT	5.0 ± 0.2	4.63 ± 0.31	4.26 ± 0.1	3.2 ± 0.4	3.49 ± 0.13	3.26 ± 0.13	3.02 ± 0.13
T_{ion} (keV) DD	4.3 ± 0.2	3.77 ± 0.2	3.7 ± 0.3	3.0 ± 0.3	3.2 ± 0.2	2.9 ± 0.3	2.2 ± 0.2
DSR (%)	4.0 ± 0.4	3.85 ± 0.41	4.13 ± 0.3	2.7 ± 0.5	3.3 ± 0.2	2.7 ± 0.19	2.9 ± 0.14
Neutron bang-time (ns)	16.41 ± 0.03	16.59 ± 0.03	16.753 ± 0.03	16.86 ± 0.03	16.49 ± 0.03	16.66 ± 0.03	16.76 ± 0.03
τ_x (ps)	152.0 ± 33	161.0 ± 34	160 ± 10	200.95 ± 10	156 ± 60	270 ± 15	225 ± 12
τ_n (ps)	156.0 ± 30	188.0 ± 33	156 ± 30	216 ± 40	180 ± 40	215 ± 40	172 ± 40
$P0_x$	37.52 ± 1.39	39.11 ± 3.16	35.78 ± 2.73	38.67 ± 5.7	42.95 ± 1.71	41.2 ± 2.18	31.05 ± 1.43
$P2/P0_x$	-0.283 ± 0.038	-0.0993 ± 0.059	-0.214 ± 0.103	-0.46 ± 0.09	-0.294 ± 0.0349	…	0.147 ± 0.035
$P3/P0_x$	-0.029 ± 0.049	0.0243 ± 0.035	0.001 ± 0.063	0.01 ± 0.12	0.0843 ± 0.03	…	-10.22 ± 0.091
$P4/P0_x$	0.0039 ± 0.021	-0.021 ± 0.036	0.0074 ± 0.031	0.15 ± 0.05	0.0496 ± 0.0525	…	-3.42 ± 0.067
$M0_x$	51.68 ± 4.1	47.34 ± 1.97	44.56 ± 1.52	53.22 ± 5.7	50.20 ± 3.32	50.38 ± 4.09	38.81 ± 1.52
$M2/M0_x$	0.0345 ± 0.03	0.092 ± 0.013	0.0713 ± 0.03	0.1 ± 0.05	0.14 ± 0.028	0.0897 ± 0.01	0.161 ± 0.026
$M3/M0_x$	0.0375 ± 0.012	0.002 ± 0.02	0.0936 ± 0.01	0.04 ± 0.08	0.0745 ± 0.021	0.1171 ± 0.06	0.0449 ± 0.02
$M4/M0_x$	0.0209 ± 0.017	0.05 ± 0.02	0.0434 ± 0.01	0.13 ± 0.14	0.0703 ± 0.028	0.0946 ± 0.02	0.0285 ± 0.01
ϕ_2(deg)	74 ± 22	84 ± 3	65 ± 8	75 ± 21	58 ± 6	98 ± 2.2	63 ± 4
ϕ_4(deg)	38 ± 8	41 ± 2	3 ± 4	1 ± 3	19 ± 3	62 ± 8	8 ± 5
$P0_{n,13-17}$	34 ± 4	32 ± 4	31 ± 4	…	38.85 ± 4	42 ± 4	30 ± 4
$P2/P0_{n,13-17}$	-0.34 ± 0.05	-0.35 ± 0.05	-0.26 ± 0.05	…	-0.58 ± 0.08	-0.18 ± 0.05	-0.03 ± 20
$P3/P0_{n,13-17}$	…	0.08 ± 0.05	0.14 ± 0.05	…	0.06 ± 0.05	…	…
$P4/P0_{n,13-17}$	0.01 ± 0.05	0.02 ± 0.05	-0.05 ± 0.05	…	0.05 ± 0.05	…	…
$P0_{n,6-12}$	50 ± 4	55 ± 4	50 ± 4	…	54.15 ± 4	73 ± 8	…
$P2/P0_{n,6-12}$	0 ± 0.05	0.01 ± 0.05	0 ± 0.08	…	0.07 ± 0.05	-0.1 ± 0.1	…
$P3/P0_{n,6-12}$	…	-0.02 ± 0.01	0.05 ± 0.01	…	0.18 ± 0.01	…	…
$P4/P0_{n,6-12}$	0.02 ± 0.01	-0.02 ± 0.01	0.06 ± 0.01	…	0.07 ± 0.01	…	…
Y_{total} ($\times 10^{15}$)	6.1	5.1	2.8	0.53	1.2	0.65	0.86

TABLE II. High-foot DT shot inferred properties.

Quantity	N131119	N130927	N130812	N130710	N130501
P_{hs} (Gbar)	127–144	129–150	85–110	50–67	58–80
E_{DT} (kJ)	9–12	10–14	7–9	6–8	7.5–10.5
E_{Fusion} (kJ)	17.2	14.4	7.9	3.4	2.4
v_{imp} (km/s)	322 ± 15	311 ± 15	307 ± 15	323 ± 15	297 ± 15

$v_{imp} \sim T_r^{1.65}$), the hot-spot shape became more oblate and toroidal. While the yield increased between N130501 and N130710, the inferred stagnation pressure did not (see Table II). (Note: shot N130530 was performed with an ice layer that was well out of specified tolerances having $m = 1$ mode "M1" of over 5 μm peak-to-valley amplitude, but tested simulation predictions that the neutron yield would decrease by half as compared to an equivalent target with the ice-layer inside specified tolerances, i.e., N130710.) In an attempt to improve hot-spot shape, shot N130802 was performed using the "+700" hohlraum geometry (see Appendix A) that previously gave improved ablator shape[20] (right frame of Fig. 4), but apparently the shape improvement did not carry over to the hot-spot and the capsule performance therefore suffered. The combined experience of N130710 and N130802 both indicated reduced efficacy of inner-beam laser propagation to the waist of the hohlraum as laser power and inner-beam path length was increased, so in order to recover better hot-spot shape control while also increasing implosion performance, efforts shifted to lower laser powers but higher laser energy implosions, with the nominal length hohlraum.

In shots N130812, N130927, and N131119, the laser power was reduced as compared to N130710, but the laser energy was increased. For these higher energy shots, the time duration between bang-time and time the laser shuts off is reduced creating a "no-coast" (<1 ns between laser shut-off and bang-time) implosion that leads to higher fuel compression and slightly higher implosion speeds as compared to "coasting" implosions (>1 ns between laser shut-off and bang-time) at the same laser power. As can be seen in Table I, the no-coast strategy was successful in increasing the implosion performance with the high-foot pulse-shape (mixing occurred in low-foot implosions under no-coast drive). Fig. 5 shows improved shape for these no-coast high-foot implosions, but the shape remained somewhat toroidal, albeit more compact toroids than was observed in N130710.

Integrated hohlraum-capsule simulations in 2D (using HYDRA[36]) are able to capture the salient characteristics of the observed implosion shapes (hot-spot and fuel shape) using a scenario where the CBET is reduced late in time during the laser pulse, thus reducing the drive on the waist of the capsule in combination with the known P_4 mode associated with the position of the laser spots in the nominal hohlraum (see Fig. 6). Inspection of the simulation in Fig. 6 shows that the reduced emission from the center of the toroidal shape is not actually a hole, but instead a thinning of the hot-spot and increased optical depth due to a collection of compressed DT fuel mass preferentially located on the poles of the implosion.

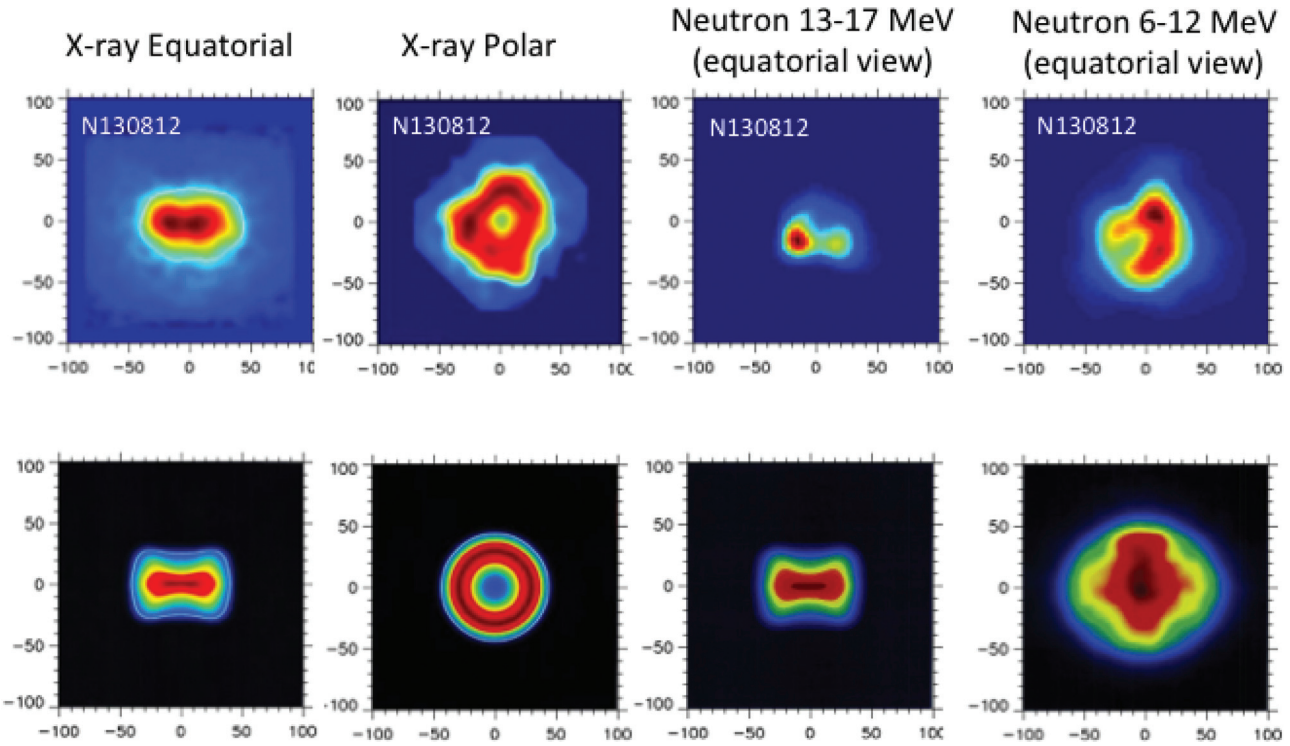

FIG. 6. From left to right are shown hot-spot images of x-ray emission equatorial view, x-ray emission polar view, direct neutrons, and indirect neutrons. The top row shows data from experiment N130812 and the bottom row shows the results from 2D integrated hohlraum capsule simulation with a time-dependent CBET that tapers off at late time in order to mimic the observed shape. Dimensions are in μm. Reprinted with permission from Phys. Rev. Lett. **112**, 055001 (2014). Copyright 2014 AIP Publishing LLC.

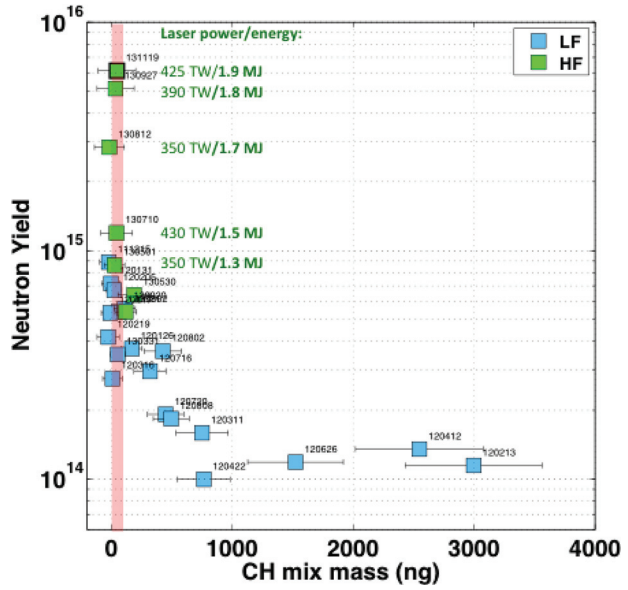

FIG. 7. For the database of high-foot (green) and low-foot (blue) shots on NIF, total neutron yield is plotted against the inferred amount of ablator mix.[37] An uncertainty band corresponding to 100 ng of mix is imposed in the figure. Laser power and energy for the key high-foot experiments are noted.

In spite of the toroidal shapes and even for the worst performing high-foot implosions, the inferred levels of CH ablator mix into the hot-spot were low (<100 ng for all but one shot, N130530 which had <200 ng of mix inferred), in contrast to low-foot implosions.[2,37,38] Fig. 7 shows a comparison of neutron yield vs. CH mix mass for all high-foot shots and a select number of low-foot shots. Note in Fig. 7 that several low-foot shots had low mix inferred—these were lower speed coasting implosions generally. Interestingly, in-spite of non-1D shape, 1D simulations of high-foot shots are in much better agreement with measured yield than low-foot shots (see Fig. 8 where yield-over-clean, YOC, from 1D HYDRA[36]

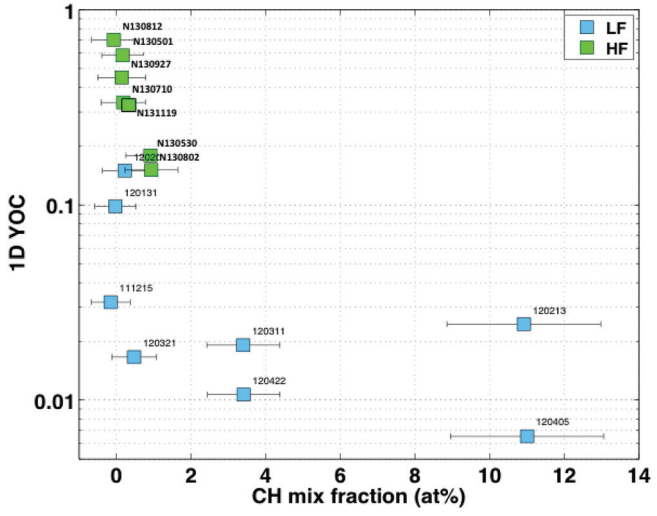

FIG. 8. 1D simulations of the implosion performance (using multi-frequency radiation drive sources that are calibrated to shock-timing and implosion trajectory data) are plotted against ablator mix fraction. High-foot results (green) show high YOC, while low-foot results are generally lower. As expected, for low-foot experiments with large mix fractions, the YOC is particularly low.

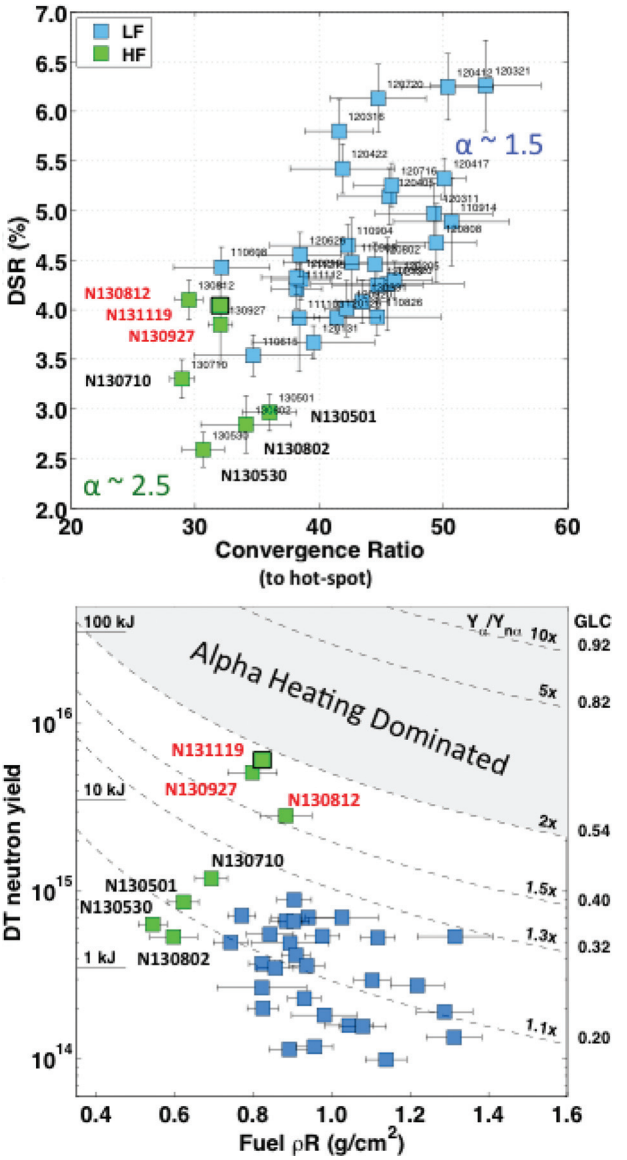

FIG. 9. (Top frame) *DSR*, a measure of $(\rho r)_{fuel}$ is plotted against hot-spot convergence ratio. (Bottom frame) total neutron yield is plotted against fuel $(\rho r)_{fuel}$. High-foot shots (green) are generally less compressed and have a higher yield than low-foot (blue) shots consistent with high-foot adiabat being higher and convergence ratio lower than low-foot shots. The three highest performing shots are highlighted with their shot number in red. Contours of yield multiplication due to alpha-particle self-heating and GLC are also shown on the right frame.

simulation is plotted against CH ablator mix fraction). Both the improved A-RT stability and reduced convergence ratio, *CR*, of the high-foot pulse-shape contribute to a more predictable implosion as measured by higher YOC.

The expected reduced hot-spot *CR* and fuel compression levels for the high-foot implosions are measured and shown in Fig. 9 (left frame). In Fig. 9, it is observed that high-foot implosions generally compress less, but there is also a considerable range of compressions/convergence within each class of either high-foot or low-foot implosions. In spite of trading off compression to gain stability, the net performance of the high-foot in terms of ignition metrics, such as generalized Lawson criteria (GLC)[39] or yield amplification due to α-particle self-heating[40] ($Y_\alpha/Y_{n\alpha}$, ratio of yield with

α-particle deposition over yield with no α-particle heat deposition), the most recent high-foot experiments are the best performing ICF implosions to date and are on the boundary of becoming α-particle self-heating dominated (Fig. 9, right frame). An α-particle self-heating dominated shot, N140120, was recently performed.

V. ENERGY BALANCE

Other important metrics about the performance of the implosions can be calculated directly from the observables coming from each experiment[7,41,42] bypassing the need to make inferences from simulations calibrated to the data. An outline of the procedure is as follows: From the measurement of T_{ion}, one can calculate the DT reaction-rate, $\langle\sigma v\rangle$, using well known expressions, e.g., Ref. 43. Reconstructing the 3D shape of the hot-spot from the equatorial and polar imaging data yields the volume of the hot-spot, V_{hs}. With the measured neutron yield, the hot-spot number density, n_{hs}, can be calculated from the fusion power density,[44] $\langle\sigma v\rangle$, V_{hs}, and the measured duration of the DT burn, τ_x or τ_n. With n_{hs} a variety of average bang-time hot-spot quantities can be derived (see Table II) such as the mass, m_{hs}, stagnation pressure, P_{hs}, areal density, $(\rho r)_{hs}$, fraction of α-particles deposited,[45] α-particle energy deposited, and internal energy, $\frac{3}{2}P_{hs}V_{hs}$. Properties of the cold fuel then follow from mass conservation and the *DSR* measurement. Accounting for x-ray losses and energy deposition due to α-particles the total energy delivered to the DT during the implosion up to bang-time, E_{DT}, can be calculated. Details of these calculations for high-foot shots N130927 and N131119 are given in Ref. 7

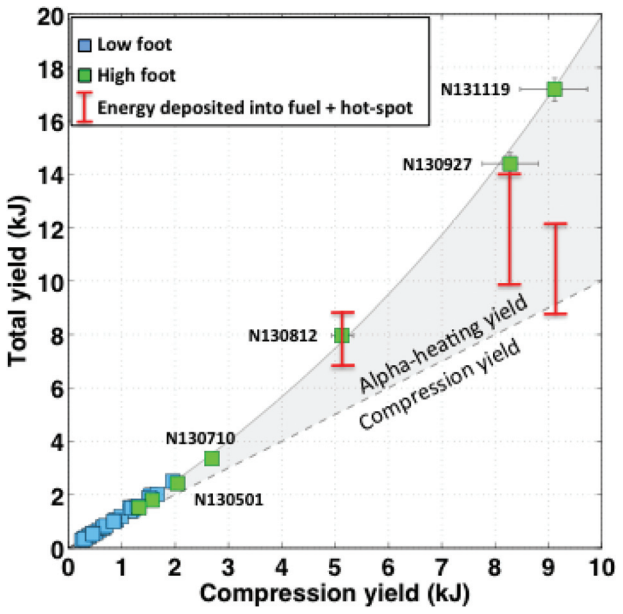

FIG. 10. Total yield vs. the yield expected from compression alone is plotted for high-foot (green) and low-foot (blue) experiments. The grey shaded region illustrates the extra amount of yield coming from alpha-particle self-heating.[41] Shown in red is the total amount of energy delivered into the DT by the implosion.[7] The last two highest performing shots, shown on this plot, exhibit $G_{fuel} > 1$ (shots subsequent to N131119, N131219, and N140120 also have $G_{fuel} > 1$).

where it is demonstrated that these shots achieved fuel gains (ratio of fusion energy produced to total energy deposited into the DT), $G_{fuel} > 1$. Table II summarizes hot-spot model energetics results for select high-foot DT shots.

Fig. 10 graphically summarizes the performance of the high-foot campaign in terms of compression yield,[41] α-particle self-heating yield, and total (hot-spot plus cold fuel) DT energy. As is clear in Fig. 10, on the last few high-foot shots, we are also seeing a significant contribution to the yield coming from alpha-particle self-heating and evidence for the "bootstrapping" required to accelerate the DT fusion burn-rate to eventually run-away ignite.

VI. CONCLUSION

High-foot implosions appear to hold promise for understanding integrated ICF physics, testing performance cliffs, and for further optimizing performance. In this first year of the campaign, many goals have been achieved. Namely, high-foot implosions obtained very high yield-over-simulated (aka YOC) and have been diagnosed to be essentially "clean" with respect to mix, even with $CR \sim 30$–35. The assertion that the high-foot pulse-shape would generate less instability growth in the ablator has been proven both indirectly, through the measured integrated implosion performance, and directly through RT growth experiments.[22,23] As of this writing, high-foot implosions hold the yield record for ICF implosions, obtaining ~26 kJ of fusion yield and have for the first time on any fusion facility achieved fuel gains in excess of unity.

Effectively, the high-foot implosion has proven, by example, that A-RT was a major issue in the performance of the NIC (i.e., low-foot) implosion. It is important to recognize that A-RT instability was likely not the only issue for NIC, however. By creating a more robust implosion with the high-foot, we are seeing other physics challenges expressed in the data that were hidden in the NIC (but suspected) because A-RT was so dominant. A key remaining challenge includes, but is not limited to, hohlraum control of low-mode shape (hot-spot and fuel) especially at higher laser powers and energies—control through $\Delta\lambda$'s appears to have reached its limit (a recent shot, N140120 using a depleted uranium hohlraum, has shown progress in this area).

Near term strategies using the high-foot involve using it as an *evolving* design, having the benefit of a working implosion as a point to perform perturbations/optimizations around. As was mentioned at the beginning of this article, stagnation pressure is key, so stagnation pressure is what needs to be optimized. Scaling of stagnation pressure with implosion speed, hot-spot shape, adiabat, and ablation pressure is known and guides future work. In particular, efforts to increase implosion speed and improve hohlraum driven shape will include using thinner ablators and using different geometry hohlraums. Fuel adiabat will be reduced either through a "medium" foot or through a more elaborate indirect drive analog of an adiabat shaping scheme.[46,47] Also, high-foot like approaches will be examined with ablators materials alternate to CH. Each of these approaches potentially gives back some of the stability gains demonstrated

with the high-foot, but it will be a matter of research to see which of the above paths provides the best way to further α-heating and, hopefully, ignition.

ACKNOWLEDGMENTS

We thank P. Albright, J. Atherton, D. Bradley, B. Burr, D. Clark, W. Goldstein, B. Goodwin, G. Gururangan, W. Hsing, O. Jones, D. Kalantar, R. Kirkwood, L. Kot, A. Hamza, J. Kilkenny, O. Landen, J. Lindl, A. Mackinnon, B. MacGowan, J. F. Meeker, N. Meezan, E. Moses, T. Parham, D. Strozzi, R. Town, C. Verdon at LLNL and NIF operations, cryogenics, and targets teams. Thanks to L. Peterson, K. Raman, and V. Smalyuk of the Hydro-growth Radiography Team for discussions on High-foot stability. Thanks to C. Wilde and P. Volegov of LANL for their contribution to the NIS system and analysis and to our other external collaborators at LANL (diagnostics), GA (targets), LLE (diagnostics), the MIT Plasma Science and Fusion Center (MRS diagnostic), CEA, and AWE. This work was performed under the auspices of the U.S. Department of Energy by Lawrence Livermore National Laboratory under Contract No. DE-AC52-07NA27344.

APPENDIX A: HIGH-FOOT CAMPAIGN SHOTS

In this appendix, we give a complete list of high-foot campaign shots, the motivation for each shot, and a brief results summary. Other shots, not directly associated with the high-foot campaign but using the high-foot pulse-shape did occur (such as A-RT instability growth[22,23] and hohlraum "view factor" experiments[48]) but are not listed here.

The campaign began with two keyhole[11,12] shots, N121023 and N121102, which provided a first look at 3-shock tuning and initial laser back-scatter information. The first result showed a slower than expected first shock (22 km/s rather than the designed speed of 28 km/s) and backscatter of 98–140 kJ of energy (84.1%–85.1% laser energy coupling to the hohlraum). The first shock speed was increased, in the second shot, to the designed speed by increasing the power in the trough of the pulse. Additionally, these shots had excellent pole-waist symmetry, as seen by the coincidence of shock merger timing at the pole and equator (see Fig. 11).

Symcaps N121130 and N130108 formed a pair of hot-spot shape tuning shots (see Fig. 12) with different hohlraum He fills. Shot N121130 used 1.45 mg/cc He fill (obtaining $P2/P0 = -0.12 \pm 0.01$ time-resolved $P2/P0 = -0.05 \pm 0.013$ time-integrated) like the two keyhole shots above, while shot N130108 used a higher He fill density of 1.6 mg/cc (obtaining $P2/P0 = 0.26 \pm 0.026$ and $P2/P0 = 0.22 \pm 0.012$ time-integrated) that became the default fill density for all subsequent high-foot shots. Some evidence for a reduced M-band environment, relative to the low-foot, was also provided by this pair of shots (see Fig. 13).

After modifying the hohlraum He fill density to 1.6 mg/cc, two more keyhole tuning shots were performed, N130122 and N130214. In addition to shock tuning data, these shots motivated a change in pulse-shape strategy in order to cope with early-time hot-electrons coming from the LEH window observed on N130122. To reduce the hot-electron flux, a low power inner beam "toe" was added to the foot of the pulse effectively by delaying the turn-on of the outer-cone beams in order allow the hohlraum's LEH window to blow down before the bulk of the laser power was delivered to the hohlraum. Due to the hot-electron strategy, the good pole-waist shock symmetry observed on earlier shots was impacted (see Fig. 14).

Shot N130303 was a 2DConA[21] shot providing ablator shape and inner ablator limb speed information and is discussed in the main text (Fig. 4). Abel inversion of the streaked radiography data obtained on shot N130409—a 1DConA[53] experiment—provided ablator center-of-mass trajectory, center-of-mass speed, and thickness information. In this case, N130409 data were consistent with pre-shot simulation (see Fig. 15). N130409 was the final tuning shot required before attempting the first high-foot DT shot, N130501,[6] at modest laser power and energy, 350 TW and 1.3 MJ, respectively.

Up through N130501, all high-foot shots had been performed in nominal length (9.425 mm) hohlraums. Due to the proximity of the outer beams on the inside of the hohlraum, implosions using this nominal length hohlraum exhibited a

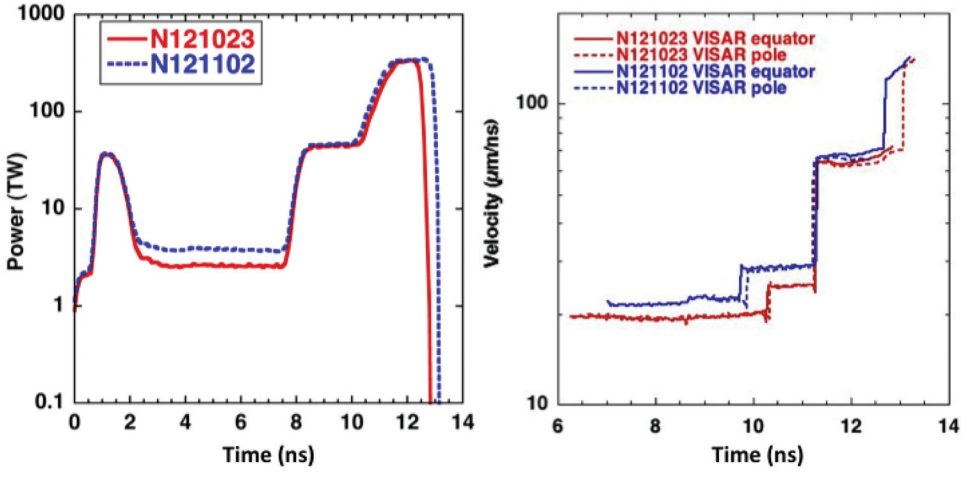

FIG. 11. (Left frame) Laser pulse-shapes for the first two high-foot shock-timing (keyhole) experiments are shown along with the resulting shock velocity histories (right frame). For each experiment, a pole and waist measurement is obtained. Since D_2 blanks the VISAR (velocity interferometer system for any reflector) diagnostic (due to shock pressure ionization), the velocity traces truncate above ~145 km/s.

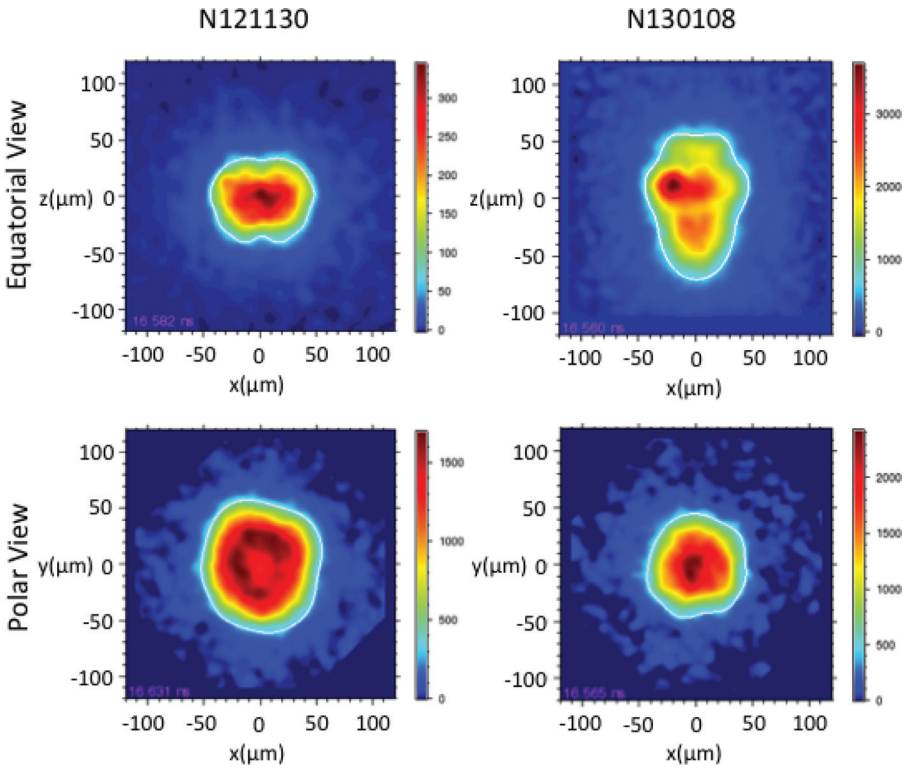

FIG. 12. Hot-spot x-ray emission from symmetry capsule (symcap) experiments shows how the shape varies with hohlraum He fill pressure with a choice of $\Delta\lambda_{23.5} = 8.5$Å and $\Delta\lambda_{30} = 7.3$Å for both shots. The upper row shows the equatorial view, while the lower row shows the polar view.

P4 mode in the ablator shape. In order to remove this P4 mode, a series of longer hohlraums with different beam pointing were developed by another group.[20]

Keyhole shots N130521 and N130726 formed a companion pair of shock timing experiments in the longer "+700" (10.125 mm) hohlraum. Shot N130522 was a re-emit experiment[49,50] in the +700 hohlraum configuration that provides early-time ("picket") capsule x-ray illumination symmetry information. Data from N130522 indicated that the cone-fraction (CF) for the +700 hohlraums was incorrect yielding a radiation asymmetry that was waist hot ($P2/P0 \sim 0.025$) and that a lower CF was required for the +700 hohlraums to prevent capsule symmetry swings later in the implosion. Translating the N130522 data to the nominal hohlraum case, using simulations, suggested that the CF of 5%–6% used was appropriate for the nominal hohlraum length. Incidental data coming from the N130522 re-emit experiment provided the first time-integrated (from 1.75–2.8 ns) hard x-ray (40 keV) images of hot-electrons (see Fig. 16)—data that can conceivably be used to estimate the amount of early-time (LEH window) hot-electrons that reach the capsule when used together with FFLEX[51,52] hot-electron data (estimates are that 5% of total picket hot electrons, as measured by FFLEX, reach the capsule).

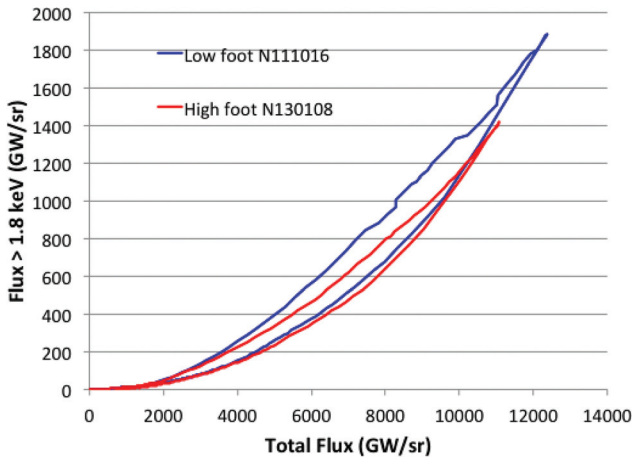

FIG. 13. Measurements of hohlraum x-ray flux above 1.8 keV indicate a slightly reduced non-Planckian component to the x-ray spectrum for a high-foot shot (red) as compared to an equivalent low-foot shot (blue). The *apparent* two curves for each shot just express the time history as the hohlraum goes from cold to hot (lower curve) then hot to cold (upper curve).

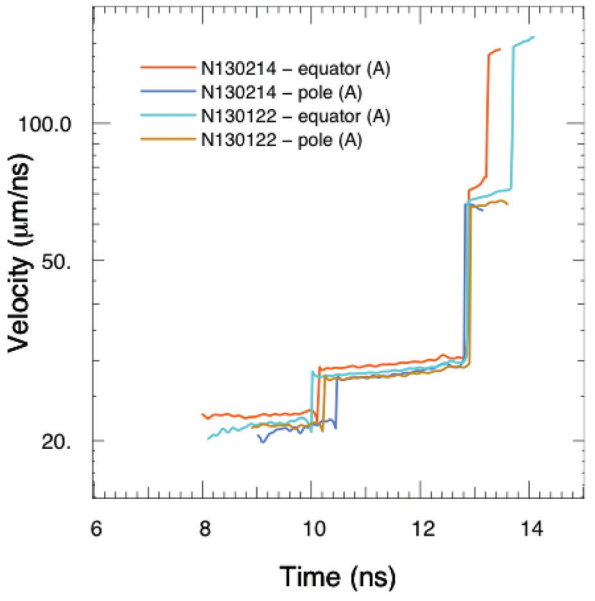

FIG. 14. Shock velocity history data are shown for high-foot experiments using a 1.6 mg/cc He hohlraum fill density.

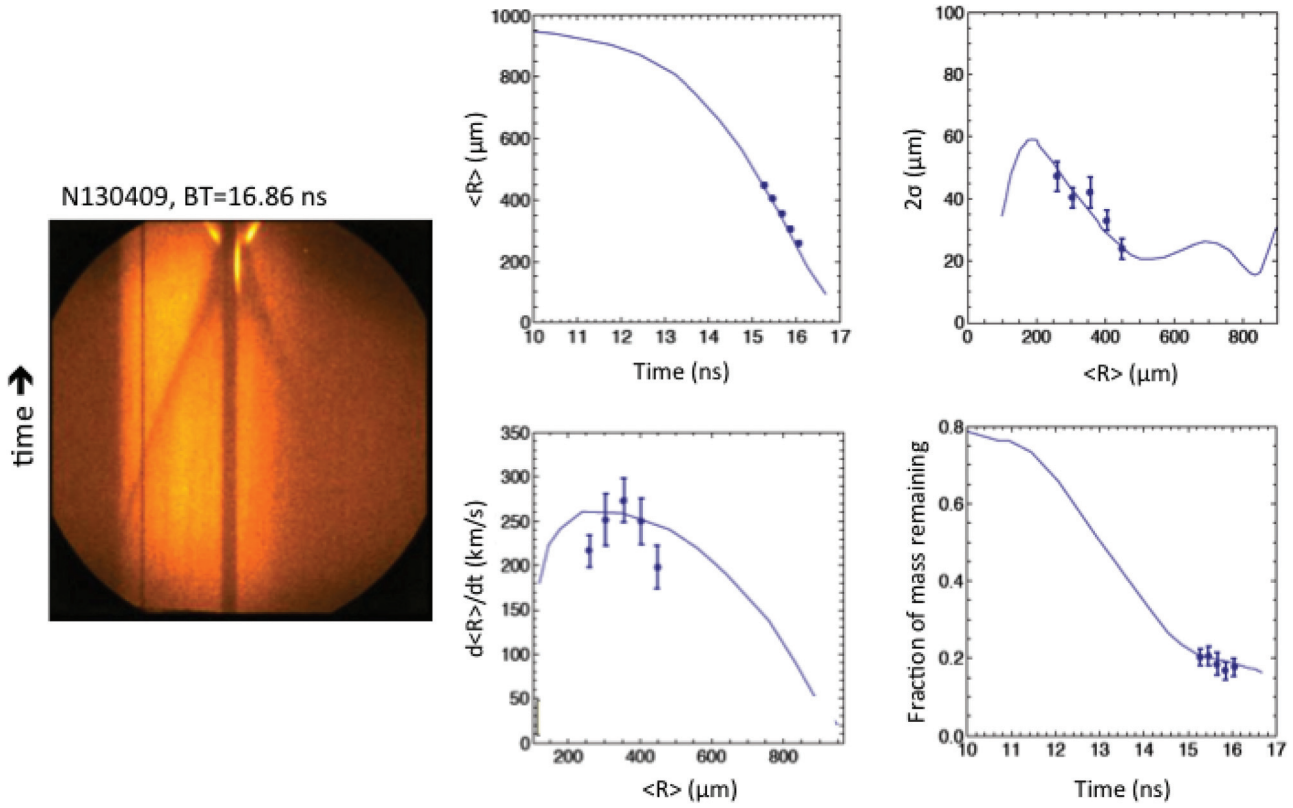

FIG. 15. Streaked radiograph data (left frame) for high-foot experiment N130409 gives ablator center-of-mass trajectory (upper center), ablator thickness (upper right), ablator center-of-mass speed (lower middle), and ablator mass remaining (lower right).

2DConA shots N130508 and N130808 are companion experiments for the longer "+700" hohlraum. These two shots were performed at 350 TW and 1.3 MJ of laser power/energy but with different laser wavelengths.[32–35] In particular, N130508 used $\Delta\lambda_{30} = 5.4$Å and $\Delta\lambda_{23.5} = 6.4$Å while N130808 used $\Delta\lambda_{30} = 7.4$Å and $\Delta\lambda_{23.5} = 8.4$Å. While these experiments did indeed demonstrate reduced P4 mode in the ablator, they also demonstrated strong negative P2 mode (oblate) shaped hot-spots that we were limited in our ability to control with CBET (see Fig. 17). Another "+700" 2DConA shot was performed with laser power/energy of 430 TW/1.5 MJ, N130730, and exhibited a close to round ablator shape but a very oblate hot-spot shape ($P2/P0 = -0.316$). An attempt was made to apply a further $\Delta\lambda$ correction to alleviate the oblate hot-spot shape before performing a +700 DT shot, N130802, but that effort was futile as the DT shot performed poorly having essentially the same hot-spot shape distortion as N130731. After shots N130802 and N130808, further efforts on the +700 hohlraum were suspended by our campaign.

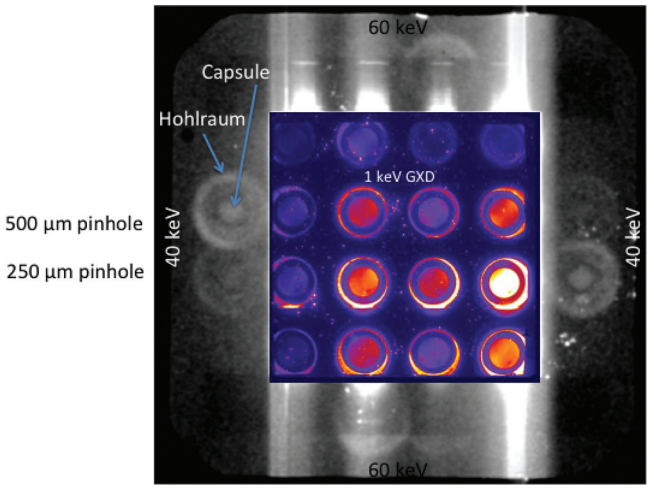

FIG. 16. Hard x-ray energy emission images (perimeter) show illumination of the capsule and hohlraum by hot-electrons. At lower energies (middle), the illumination of the capsule by the Planckian part of the radiation field in the hohlraum is obtained.

In parallel with the attempt to utilize the +700 hohlraum, perturbations on the successful N130501 shot were performed to explore the nearby parameter space and test the veracity of our simulation predictions. Shot N130530 was meant to test higher implosion speeds using a 430 TW/1.5 MJ pulse-shape, but it also had a large (~5 μm peak-to-valley) $m = 1$ perturbation in the ice layer, so it instead tested a simulation prediction that such a perturbation in the DT ice layer would reduce the yield by 50%. A repeat of shot N130530, but with an in-spec DT ice layer, was performed in shot N130710[6] which showed increased yield, but no increase in P_{stag} due to increased hot-spot shape distortion. DT layer shots N130812, N130927, and N131119 then built upon N130501 by using lower peak power, but more laser energy—a so-called "no coast" implosion mode.[6,7]

In an effort to increase implosion speed, while maintaining lower laser power where better hot-spot shape control was experienced, the campaign recently embarked upon a series of thinner (by 10%) ablator shots ("T-1" thickness, 175 μm)

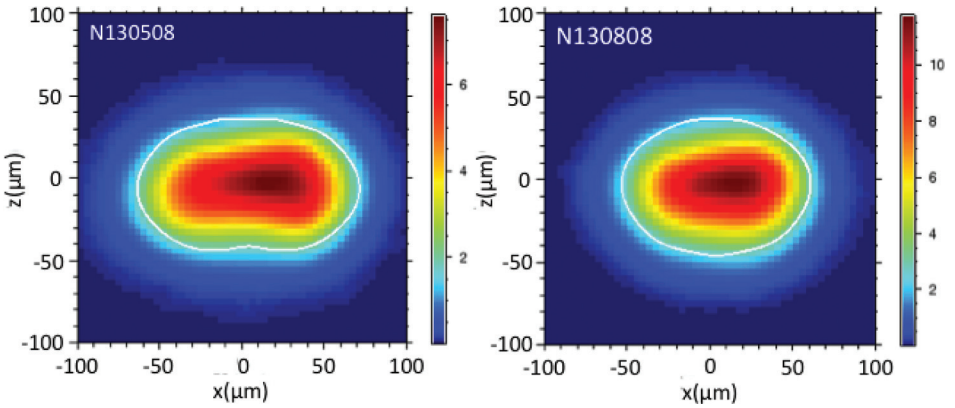

FIG. 17. Oblate hot-spot shapes (equatorial view) from two experiments with different $\Delta\lambda$'s but identical laser power and energy are shown for experiments performed in the +700 hohlraum. $P0$ changed from $55.89 \pm 1.96\,\mu$m to $50.71 \pm 2.1\,\mu$m and $P2/P0$ changed from -0.333 ± 0.026 to -0.217 ± 0.011 going from N130508 to N130808.

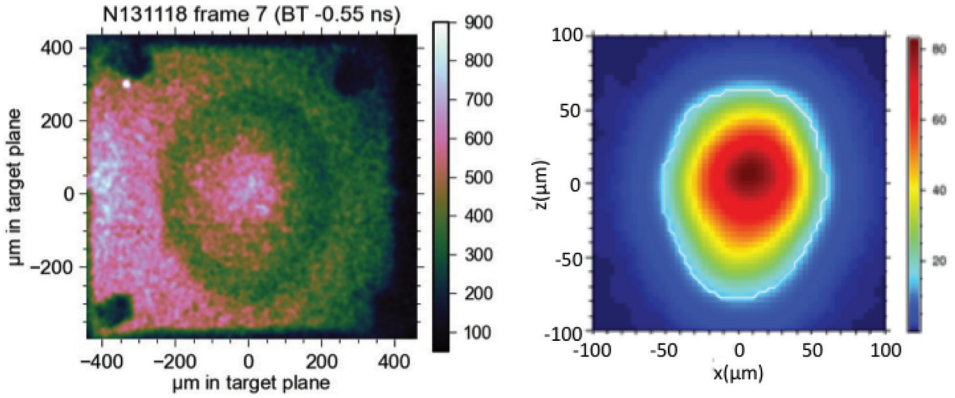

FIG. 18. The ablator shape are peak velocity (left frame) and hot-spot shape at bang-time (right frame) are shown for shot N131118 (thinner ablator in a nominal hohlraum at 350 TW and 1.63 MJ of laser power and energy).

in 2DConA N131118, keyhole N131126, and DT layer shot N131219. N131118 used $\Delta\lambda_{30} = 7.5$Å and $\Delta\lambda_{23.5} = 8.2$Å and achieved a slightly prolate ($P2/P0 = 0.14 \pm 0.02$) ablator shape and prolate ($P2/P0 = 0.17 \pm 0.02$) hot-spot shape (Fig. 18) indicating improved inner beam propagation to the waist of the hohlraum at late-time as compared to the T0 thickness (195 μm) capsules. The implosion speed on N131118 was measured to be 349 ± 20 km/s using a 350 TW and 1.63 MJ laser pulse. The DD yield and measured T_{ion} from the DHe_3 filled capsule was high compared to the database of all previous shots being 1.1×10^{12} and 3.2 keV, respectively.

In order to round out the hot-spot shape for the following T-1 high-foot implosions, the laser wavelengths were reset to $\Delta\lambda_{30} = 6.2$Å and $\Delta\lambda_{23.5} = 6.9$Å reducing the degree of CBET. With this change, keyhole shot N131126 indicated a 500 ps lengthening of the duration of the foot part of the pulse-shape in order to obtain the proper merge depth for the 1st and 2nd shock for DT layer shot N131219. As of this writing, shot N131219 obtained $Y_{13-15} = (3.0 \pm 0.055) \times 10^{15}$, $DSR = 4.4 \pm 0.2\%$, $T_{ion}(DT) = 5.1 \pm 0.1$ keV, and $T_{ion}(DD) = 4.5 \pm 0.2$ keV with no indications of mix.

[1]E. I. Moses, IEEE Trans. Plasma Sci. **38**, 684 (2010).
[2]M. J. Edwards, P. K. Patel, J. D. Lindl, L. J. Atherton, S. H. Glenzer, S. W. Haan, J. D. Kilkenny, O. L. Landen, E. I. Moses, A. Nikroo, R. Petrasso, T. C. Sangster, P. T. Springer, S. Batha, R. Benedetti, L. Bernstein, R. Betti, D. L. Bleuel, T. R. Boehly, D. K. Bradley, J. A. Caggiano, D. A. Callahan, P. M. Celliers, C. J. Cerjan, K. C. Chen, D. S. Clark, G. W. Collings, E. L. Dewald, L. Divol, S. Dixit, T. Döppner, D. H. Edgell, J. E. Fair, M. Farrell, R. J. Fortner, J. Frenje, M. G. Gatu Johnson, E. Giraldez, V. Yu. Glebov, G. Grim, B. A. Hammel, A. V. Hamza, D. R. Harding, S. P. Hatchett, N. Hein, H. W. Herrmann, D. Hicks, D. E. Hinkel, M. Hoppe, W. W. Hsing, N. Izumi, B. Jacoby, O. S. Jones, D. Kalantar, R. Kauffman, J. L. Kline, J. P. Knauer, J. A. Koch, B. J. MacGowen, A. J. Mackinnon, A. Macphee, E. R. Mapoles, M. M. Marinak, M. Mauldin, P. W. McKenty, N. Meezan, P. A. Michel, J. Milovich, J. D. Moody, M. Moran, D. H. Munro, C. L. Olsen, K. Opachich, A. E. Park, T. Parham, H.-S. Park, J. E. Ralph, S. P. Regan, B. Remington, H. Rinderknecht, H. F. Robey, M. Rosen, S. Ross, J. D. Salmonson, J. Sater, D. H. Schneider, F. H. Séguin, S. M. Sepke, D. A. Shaughnessy, V. A. Smalyuk, B. K. Spears, C. Stoeckl, W. Stoeffl, L. Suter, C. A. Thomas, R. Tommasini, R. P. Town, S. V. Weber, P. J. Wegner, K. Widmann, M. Wilke, D. C. Wilson, C. B. Yeamans, and A. Zylstra, Phys Plasmas **20**, 070501 (2013).
[3]J. D. Lindl and E. I. Moses, Phys. Plasmas **18**, 050901 (2011).
[4]V. N. Goncharov and O. A. Hurricane, "Panel 3 Report: Implosion Hydrodynamics" LLNL Report No. LLNL-TR-562104, 2012. Op cit. "Science of Fusion Ignition on NIF Workshop, 22–24 May, 2012" LLNL Report No. LLNL-TR-570412, 2012.
[5]T. R. Dittrich, O. A. Hurricane, D. A. Callahan, E. L. Dewald, T. Döppner, D. E. Hinkel, L. F. Berzak Hopkins, S. LePape, T. Ma, J. Milovich, J. C. Moreno, P. K. Patel, H.-S. Park, B. A. Remington, and J. Salmonson, Phys. Rev. Lett. **112**, 055002 (2014).
[6]H.-S. Park, O. A. Hurricane, D. A. Callahan, D. T. Casey, E. L. Dewald, T. R. Dittrich, T. Döppner, D. E. Hinkel, L. F. Berzak Hopkins, S. Le Pape, T. Ma, P. K. Patel, B. A. Remington, H. F. Robey, and J. D. Salmonson, Phys. Rev. Lett. **112**, 055001 (2014).
[7]O. A. Hurricane, D. A. Callahan, D. T. Casey, P. M. Celliers, C. Cerjan, E. L. Dewald, T. R. Dittrich, T. Döppner, D. E. Hinkel, L. F. Berzak Hopkins, J. L. Kline, S. LePape, T. Ma, A. G. MacPhee, J. L. Milovich, A. Pak, H.-S. Park, P. K. Patel, B. A. Remington, J. D. Salmonson, P. T. Springer, and R. Tommasini, Nature **506**, 343–348 (2014).
[8]S. E. Bodner, Phys. Rev. Lett. **33**, 761–764 (1974).
[9]S. H. Glenzer, D. A. Callahan, A. J. Mackinnon, J. L. Kline, G. Grim, E. T. Alger, R. L. Berger, L. A. Bernstein, R. Betti, D. L. Bleuel, T. R. Boehly, D. K. Bradley, S. C. Burkhart, R. Burr, J. A. Caggiano, C. Castro, D. T. Casey, C. Choate, D. S. Clark, P. M. Celliers, C. J. Cerjan, G. W. Collings, E. L. Dewald, P. DiNiicola, J. M. DiNicola, L. Divol, S. Dixit, T. Döppner, R. Dylla-Spears, E. Dzenitis, M. Eckart, G. Erbert, D. Farley, J. E. Fair, D. Fittinghoff, M. Frank, L. J. A. Frenje, S. Friedrich, M. G. Gatu Johnson, C. Gibson, E. Giraldez, V. Yu. Glebov, S. Glenn, N. Guler, S. W.

Haan, B. J. Haid, B. A. Hammel, A. V. Hamza, C. A. Haynam, G. M. Heestand, M. Hermann, H. W. Herrmann, D. G. Hicks, D. E. Hinkel, J. P. Holder, D. M. Holunda, J. B. Horner, W. W. Hsing, H. Huang, N. Izumi, M. Jackson, O. S. Jones, D. H. Kalantar, R. Kauffman, J. D. Kilkenny, R. Kirkwood, J. Klingmann, T. Kohut, J. P. Knauer, J. A. Koch, B. Kozioziemski, G. A. Kyrala, A. L. Kritcher, J. Kroll, K. La Fortune, R. Lowe-Webb, T. Ma, J. McNaney, A. G. Macphee, T. N. Malsbury, E. Mapoles, C. D. Marshall, N. B. Meezan, F. Merrill, P. Michel, J. D. Moody, A. S. Moore, M. Moran, K. A. Moreno, D. H. Munro, B. R. Nathan, A. Nikroo, R. E. Olsen, C. D. Orth, A. E. Pak, P. K. Patel, T. Parham, R. Petrasso, J. E. Ralph, S. P. Regan, H. Rinderknecht, H. F. Robey, J. S. Ross, M. D. Rosen, R. Sacks, J. D. Salmonson, R. Saunders, J. Sater, C. Sangster, M. B. Schneider, F. H. Séguin, S. M. Sepke, M. J. Shaw, B. K. Spears, P. T. Springer, W. Stoeffl, L. J. Suter, C. A. Thomas, R. Tommasini, R. P. J. Town, C. Walters, S. Weaver, S. V. Weber, P. J. Wegner, P. K. Whitman, K. Widmann, C. C. Widmayer, C. H. Wilde, D. C. Wilson, B. Van Wonterghem, B. J. MacGowan, L. J. Atherton, M. J. Edwards, and E. I. Moses, Phys. Plasmas **19**, 056318 (2012).

[10]S. W. Haan, J. D. Lindl, D. A. Callahan, D. S. Clark, J. D. Salmonson, B. A. Hammel, L. J. Atherton, R. C. Cook, M. J. Edwards, S. Glenzer, A. V. Hamza, S. P. Hatchet, M. C. Herrmann, D. E. Hinkel, D. D. Ho, H. Huang, O. S. Jones, J. Klien, G. Kyrala, O. L. Landen, B. J. MacGowan, M. M. Marinak, D. D. Meyerhofer, J. L. Milovich, K. A. Moreno, E. I. Moses, D. H. Munro, A. Nikroo, R. E. Olsen, K. Peterson, S. M. Pollaine, J. E. Ralph, H. F. Robey, B. K. Spears, P. T. Springer, L. J. Suter, C. A. Thomas, R. P. Town, R. Vesey, S. V. Weber, H. L. Wilkens, and D. C. Wilson, Phys. Plasmas **18**, 051001 (2011).

[11]H. F. Robey, T. R. Boehly, P. M. Celliers, J. H. Eggert, D. Hicks, R. F. Smith, R. Collins, M. W. Bowers, K. G. Krauter, P. S. Datte, D. H. Munro, J. L. Milovich, O. S. Jones, P. A. Michel, C. A. Thomas, R. E. Olson, S. Pollaine, R. P. J. Town, S. Haan, D. Callahan, D. Clark, J. Edwards, J. L. Kline, S. Dixit, M. B. Schneider, E. L. Dewald, K. Widmann, J. D. Moody, T. Döppner, H. B. Radousky, A. Throop, D. Kalantar, P. DiNicola, A. Nikroo, J. J. Kroll, A. V. Hamza, J. B. Horner, S. D. Bhandarkar, E. Dzenitis, E. Alger, E. Giraldez, C. Castro, K. Moreno, C. Haynam, K. N. LaFortune, C. Widmayer, M. Shaw, K. Jancaitis, T. Parham, D. M. Holunga, C. F. Walters, B. Haid, E. R. Mapoles, J. Sater, C. R. Gibson, T. Malsbury, J. Fair, D. Trummer, K. R. Coffee, B. Burr, L. V. Berzins, C. Choate, S. J. Brereton, S. Azevedo, H. Chandrasekaran, D. C. Eder, N. D. Masters, A. C. Fisher, P. A. Sterne, B. K. Young, O. L. Landen, B. M. Van Wonterghem, B. J. MacGowan, J. Atherton, J. D. Lindl, D. D. Meyerhofer, and E. Moses, Phys. Plasmas **19**, 042706 (2012).

[12]H. F. Robey, P. M. Celliers, J. L. Kline, A. J. Mackinnon, T. R. Boehly, O. L. Landen, J. H. Eggert, D. Hicks, S. Le Pape, D. R. Farley, M. W. Bowers, K. G. Krauter, D. H. Munro, O. S. Jones, J. L. Milovich, D. Clark, B. K. Spears, R. P. J. Town, S. W. Haan, S. Dixit, M. B. Schneider, E. L. Dewald, K. Widmann, J. D. Moody, T. Döppner, H. B. Radousky, A. Nikroo, J. J. Kroll, A. V. Hamza, J. B. Horner, S. D. Bhandarkar, E. Dzenitis, E. Alger, E. Giraldez, C. Castro, K. Moreno, C. Haynam, K. N. LaFortune, C. Widmayer, M. Shaw, K. Jancaitis, T. Parham, D. M. Holunga, C. F. Walters, B. Haid, T. Malsbury, D. Trummer, K. R. Coffee, B. Burr, L. V. Berzins, C. Choate, S. J. Brereton, S. Azevedo, H. Chandrasekaran, B. K. Young, M. J. Edwards, B. M. Van Wonterghem, B. J. MacGowan, J. Atherton, J. D. Lindl, D. D. Meyerhofer, and E. Moses, Phys. Rev. Lett. **108**, 215004 (2012).

[13]V. N. Goncharov, T. C. Sangster, R. Epstein, S. X. Hu, I. V. Igumenshchev, D. H. Froula, R. L. McCrory, D. D. Meyerhofer, P. B. Radha, W. Seka, S. Skupsky, C. Stoeckl, D. T. Casey, J. A. Frenje, and M. Gatu-Johnson, in *Bulletin of the 54th Annual Meeting of the American Physical Society Division of Plasma Physics* (2012), Paper No. TC1.0247.

[14]T. C. Sangster, V. N. Goncharov, R. Betti, P. B. Radha, T. R. Boehly, D. T. Casey, T. J. B. Collins, R. S. Craxton, J. A. Delettrez, D. H. Edgell, R. Epstein, C. J. Forrest, J. A. Frenje, D. H. Froula, M. Gatu-Johnson, Y. Yu. Glebov, D. R. Harding, M. Hohenberger, S. X. Hu, I. V. Igumenshchev, R. Janezic, J. H. Kelly, T. J. Kessler, C. Kingsley, T. Z. Kosc, J. P. Knauer, S. J. Loucks, J. A. Marozas, F. J. Marshall, A. V. Maximov, R. L. McCrory, P. W. McKenty, D. D. Meyerhofer, D. T. Michel, J. F. Myatt, R. D. Petrasso, S. P. Regan, W. Seka, W. T. Shmayda, R. W. Short, A. Shvydky, S. Skupsky, J. M. Soures, C. Stoeckl, W. Theobald, V. Versteeg, B. Yaakobi, and J. D. Zuegel, Phys. Plasmas **20**, 056317 (2013).

[15]R. Betti, V. N. Goncharov, R. L. McCrory, and C. P. Verdon, Phys. Plasmas **5**, 1446–1454 (1998).

[16]G. Bazan, in *Proceedings from the 2nd International Workshop on Laboratory Astrophysics with Intense Lasers*, edited by B. A. Remington (Lawrence Livermore National Laboratory, Livermore, 1998), UCRL-ID-131978, pp. 42–63.

[17]R. M. Darlington, T. L. McAbee, and G. Rodrigue, Comput. Phys. Commun. **135**, 58 (2001).

[18]D. S. Clark, D. E. Hinkel, D. C. Eder, O. S. Jones, S. W. Haan, B. A. Hammel, M. M. Marinak, J. L. Milovich, H. F. Robey, L. J. Suter *et al.*, Phys. Plasmas **20**, 056318 (2013).

[19]J. Lindl, Phys. Plasmas **2**, 3933–4024 (1995).

[20]R. P. J. Town, D. K. Bradley, A. Kritcher, O. S. Jones, J. R. Rygg, R. Tommasini, M. Barrios, L. R. Benedetti, L. F. Berzak Hopkins, P. M. Celliers, T. Döppner, E. L. Dewald, D. C. Eder, J. E. Field, S. M. Glenn, N. Izumi, S. W. Haan, S. F. Khan, J. L. Kline, G. A. Kyrala, T. Ma, J. L. Milovich, J. D. Moody, S. R. Nagel, A. Pak, J. L. Peterson, H. F. Robey, J. S. Ross, R. H. H. Scott, B. K. Spears, M. J. Edwards, J. D. Kilkenny, and O. L. Landen, Phys. Plasmas **21**, 056313 (2014).

[21]J. R. Rygg, O. S. Jones, J. E. Field, M. A. Barrios, L. R. Benedetti, G. W. Collins, D. C. Eder, M. J. Edwards, J. L. Kline, J. J. Kroll, O. L. Landen, T. Ma, A. Pak, L. Peterson, K. Raman, R. P. J. Town, and D. K. Bradley, "2D x-ray radiography of imploding capsules at the National Ignition Facility," Phys. Rev. Lett. (to be published).

[22]D. T. Casey, V. A. Smalyuk, K. S. Raman, J. L. Peterson, L. Berzak Hopkins, D. A. Callahan, D. S. Clark, E. L. Dewald, T. R. Dittrich, S. W. Haan, D. E. Hinkel, D. Hoover, O. A. Hurricane, J. J. Kroll, O. L. Landen, A. S. Moore, A. Nikroo, H.-S. Park, B. A. Remington, H. F. Robey, J. R. Rygg, J. D. Salmonson, and K. Widmann, "Reduced instability growth with high adiabat ("high-foot") implosions at the National Ignition Facility," Phys. Rev. Lett. (submitted).

[23]K. S. Raman, V. A. Smalyuk, D. T. Casey, S. W. Haan, O. A. Hurricane, J. L. Peterson, B. A. Remington, H. F. Robey, D. S. Clark, B. A. Hammel, D. E. Hoover, J. J. Kroll, O. L. Landen, M. Marinak, D. H. Munro, A. Nikroo, K. J. Peterson, and J. Salmonson, "An in-flight radiography platform to measure hydrodynamic instability growth in inertial confinement fusion capsules at the National Ignition Facility," Phys. Plasmas (submitted).

[24]V. Yu. Glebov, D. D. Meyerhofer, T. C. Sangster, C. Stoeckl, S. Roberts, C. A. Barrera, J. R. Celeste, C. J. Cerjan, L. S. Dauffy, D. C. Eder, R. L. Griffith, S. W. Haan, B. A. Hammel, S. P. Hatchett, N. Izumi, J. R. Kimbrough, J. A. Koch, O. L. Landen, R. A. Lerche, B. J. MacGowan, M. J. Moran, E. W. Ng, T. W. Phillips, P. M. Song, R. Tommasini, B. K. Young, S. E. Caldwell, G. P. Grim, S. C. Evans, J. M. Mack, T. J. Sedillo, M. D. Wilke, D. C. Wilson, C. S. Young, D. Casey, J. A. Frenje, C. K. Li, R. D. Petrasso, F. H. Sguin, J. L. Bourgade, L. Disdier, M. Houry, I. Lantuejoul, O. Landoas, G. A. Chandler, G. W. Cooper, R. J. Leeper, R. E. Olson, C. L. Ruiz, M. A. Sweeney, S. P. Padalino, C. Horsfield, and B. A. Davis, Rev. Sci. Instrum. **77**, 10E715 (2006).

[25]D. L. Bleuel, C. B. Yeamans, L. A. Bernstein, R. M. Bionta, J. A. Caggiano, D. T. Casey, G. W. Cooper, O. B. Drury, J. A. Frenje, C. A. Hagmann, R. Hatarik, J. P. Knauer, M. Gatu Johnson, K. M. Knittel, R. J. Leeper, J. M. McNaney, M. Moran, C. L. Ruiz, and D. H. G. Schneider, Rev. Sci. Instrum. **83**, 10D313 (2012).

[26]M. Gatu Johnson, J. A. Frenje, D. T. Casey, C. K. Li, F. H. Sguin, R. Petrasso, R. Ashabranner, R. M. Bionta, D. L. Bleuel, E. J. Bond, J. A. Caggiano, A. Carpenter, C. J. Cerjan, T. J. Clancy, T. Döppner, M. J. Eckart, M. J. Edwards, S. Friedrich, S. H. Glenzer, S. W. Haan, E. P. Hartouni, R. Hatarik, S. P. Hatchett, O. S. Jones, G. Kyrala, S. Le Pape, R. A. Lerche, O. L. Landen, T. Ma, A. J. MacKinnon, M. A. McKernan, M. J. Moran, E. Moses, D. H. Munro, J. McNaney, H. S. Park, J. Ralph, B. Remington, J. R. Rygg, S. M. Sepke, V. Smalyuk, B. Spears, P. T. Springer, C. B. Yeamans, M. Farrell, D. Jasion, J. D. Kilkenny, A. Nikroo, R. Paguio, J. P. Knauer, V. Yu. Glebov, T. C. Sangster, R. Betti, C. Stoeckl, J. Magoon, M. J. Shoup III, G. P. Grim, J. Kline, G. L. Morgan, T. J. Murphy, R. J. Leeper, C. L. Ruiz, G. W. Cooper, and A. J. Nelson, Rev. Sci. Instrum. **83**, 10D308 (2012).

[27]B. K. Spears, private communication (2013).

[28]T. Ma, N. Izumi, R. Tommasini, D. K. Bradley, P. Bell, C. J. Cerjan, S. Dixit, T. Döppner, O. Jones, J. L. Kline, G. Kyrala, O. L. Landen, S. LePape, A. J. Mackinnon, H.-S. Park, P. K. Patel, R. R. Prasad, J. Ralph, S. P. Regan, V. A. Smalyuk, P. T. Springer, L. Suter, R. P. J. Town, S. V. Weber, and S. H. Glenzer, Rev. Sci. Instrum. **83**, 10E115 (2012).

[29]F. E. Merrill, D. Bower, R. Buckles, D. D. Clark, C. R. Danly, O. B. Drury, J. M. Dzenitis, V. E. Fatherley, D. N. Fittinghoff, R. Gallegos, G. P. Grim, N. Guler, E. N. Loomis, S. Lutz, R. M. Malone, D. D. Martinson,

D. Mares, D. J. Morley, G. L. Morgan, J. A. Oertel, I. L. Tregillis, P. L. Volegov, P. B. Weiss, C. H. Wilde, and D. C. Wilson, Rev. Sci. Instrum. **83**, 10D317 (2012).
[30]G. P. Grim, N. Guler, F. E. Merrill, G. L. Morgan, C. R. Danly, P. L. Volegov, C. H. Wilde, D. C. Wilson, D. S. Clark, D. E. Hinkel, O. S. Jones, K. S. Raman, N. Izumi, D. N. Fittinghoff, O. B. Drury, E. T. Alger, P. A. Arnold, R. C. Ashabranner, L. J. Atherton, M. A. Barrios, S. Batha, P. M. Bell, L. R. Benedetti, R. L. Berger, L. A. Bernstein, L. V. Berzins, R. Betti, S. D. Bhandarkar, R. M. Bionta, D. L. Bleuel, T. R. Boehly, E. J. Bond, M. W. Bowers, D. K. Bradley, G. K. Brunton, R. A. Buckles, S. C. Burkhart, R. F. Burr, J. A. Caggiano, D. A. Callahan, D. T. Casey, C. Castro, P. M. Celliers, C. J. Cerjan, G. A. Chandler, C. Choate, S. J. Cohen, G. W. Collins, G. W. Cooper, J. R. Cox, J. R. Cradick, P. S. Datte, E. L. Dewald, P. Di. Nicola, J. M. Di Nicola, L. Divol, S. N. Dixit, R. Dylla-Spears, E. G. Dzenitis, M. J. Eckart, D. C. Eder, D. H. Edgell, M. J. Edwards, J. H. Eggert, R. B. Ehrlich, G. V. Erbert, J. Fair, D. R. Farley, B. Felker, R. J. Fortner, J. A. Frenje, G. Frieders, S. Friedrich, M. Gatu-Johnson, C. R. Gibson, E. Giraldez, V. Y. Glebov, S. M. Glenn, S. H. Glenzer, G. Gururangan, S. W. Haan, K. D. Hahn, B. A. Hammel, A. V. Hamza, E. P. Hartouni, R. Hatarik, S. P. Hatchett, C. Haynam, M. R. Hermann, H. W. Herrmann, D. G. Hicks, J. P. Holder, D. M. Holunga, J. B. Horner, W. W. Hsing, H. Huang, M. C. Jackson, K. S. Jancaitis, D. H. Kalantar, R. L. Kauffman, M. I. Kauffman, S. F. Khan, J. D. Kilkenny, J. R. Kimbrough, R. Kirkwood, J. L. Kline, J. P. Knauer, K. M. Knittel, J. A. Koch, T. R. Kohut, B. J. Kozioziemski, K. Krauter, G. W. Krauter, A. L. Kritcher, J. Kroll, G. A. Kyrala, K. N. La Fortune, G. LaCaille, L. J. Lagin, T. A. Land, O. L. Landen, D. W. Larson, D. A. Latray, R. J. Leeper, T. L. Lewis, S. LePape, J. D. Lindl, R. R. Lowe-Webb, T. Ma, B. J. MacGowan, A. J. MacKinnon, A. G. MacPhee, R. M. Malone, T. N. Malsbury, E. Mapoles, C. D. Marshall, D. G. Mathisen, P. McKenty, J. M. McNaney, N. B. Meezan, P. Michel, J. L. Milovich, J. D. Moody, A. S. Moore, M. J. Moran, K. Moreno, E. I. Moses, D. H. Munro, B. R. Nathan, A. J. Nelson, A. Nikroo, R. E. Olson, C. Orth, A. E. Pak, E. S. Palma, T. G. Parham, P. K. Patel, R. W. Patterson, R. D. Petrasso, R. Prasad, J. E. Ralph, S. P. Regan, H. Rinderknecht, H. F. Robey, G. F. Ross, C. L. Ruiz, F. H. Sguin, J. D. Salmonson, T. C. Sangster, J. D. Sater, R. L. Saunders, M. B. Schneider, D. H. Schneider, M. J. Shaw, N. Simanovskaia, B. K. Spears, P. T. Springer, C. Stoeckl, W. Stoeffl, L. J. Suter, C. A. Thomas, R. Tommasini, R. P. Town, A. J. Traille, B. Van Wonterghem, R. J. Wallace, S. Weaver, S. V. Weber, P. J. Wegner, P. K. Whitman, K. Widmann, C. C. Widmayer, R. D. Wood, B. K. Young, R. A. Zacharias, and A. Zylstra, Phys. Plasmas **20**, 056320 (2013).
[31]P. Volegov, C. R. Danly, D. N. Fittinghoff, G. P. Grim, N. Guler, N. Izumi, T. Ma, F. E. Merrill, A. L. Warrick, C. H. Wilde, and D. C. Wilson, Rev. Sci. Instrum. **85**, 023508 (2014).
[32]P. Michel, L. Divol, E. A. Williams, S. Weber, C. A. Thomas, D. A. Callahan, S. W. Haan, J. D. Salmonson, S. Dixit, D. E. Hinkel, M. J. Edwards, B. J. MacGowan, J. D. Lindl, S. H. Glenzer, and L. J. Suter, Phys. Rev. Lett. **102**, 025004 (2009).
[33]P. Michel, S. H. Glenzer, L. Divol, D. K. Bradley, D. Callahan, S. Dixit, S. Glenn, D. Hinkel, R. K. Kirkwood, J. L. Kline, W. L. Kruer, G. A. Kryala, S. LePape, N. B. Meezan, R. Town, K. WIdmann, E. A. Williams, B. J. MacGowan, J. Lindl, and L. J. Suter, Phys. Plasmas **17**, 056305 (2010).
[34]J. D. Moody, P. Michel, L. Divol, R. L. Berger, E. Bondi, D. K. Bradley, D. A. Callahan, E. L. Dewald, S. Dixit, M. J. Edwards, S. Glenn, A. Hamza, C. Haynam, D. E. Hinkel, N. Izumi, O. Jones, J. D. Kilkenny, R. K. Kirkwood, J. L. Kline, W. L. Kruer, G. A. Kyrala, O. L. Landen, S. LePape, J. D. Lindl, B. J. MacGowen, N. B. Meezan, A. Nikroo, M. D. Rosen, M. B. Schneider, D. J. Strozzi, L. J. Suter, C. A. Thomas, R. P. J. Town, K. Widmann, E. A. Williams, L. J. Atherton, S. H. Glenzer, and E. I. Moses,, Nat. Phys. **8**, 344 (2012).
[35]D. A. Callahan, N. B. Meezan, S. H. Glenzer, A. J. Mackinnon, L. R. Benedetti, D. K. Bradley, J. R. Celeste, P. M. Celliers, S. N. Dixit, T. Döppner, E. G. Dzenitis, S. Glenn, S. W. Haan, C. A. Haynam, D. G. Hicks, D. E. Hinkel, O. S. Jones, O. L. Landen, R. A. London, A. G. MacPhee, P. A. Michel, J. D. Moody, J. E. Ralph, H. F. Robey, M. D. Rosen, M. B. Schneider, D. J. Strozzi, L. J. Suter, R. P. J. Town, K. Widmann, E. A. Williams, M. J. Edwards, B. J. MacGowan, J. D. Lindl, L. J. Atherton, G. A. Kyrala, J. L. Kline, R. E. Olson, D. Edgell, S. P. Regan, A. Nikroo, H. Wilkins, J. D. Kilkenny, and A. S. Moore, Phys. Plasmas **19**, 056305 (2012).
[36]M. M. Marinak, G. D. Kerbel, N. A. Gentile, O. Jones, D. Munro, S. Pollaine, T. R. Dittrich, and S. W. Haan, Phys. Plasmas **8**, 2275 (2001).
[37]T. Ma, P. K. Patel, N. Izumi, P. T. Springer, M. H. Key, L. J. Atherton, L. R. Benedetti, D. K. Bradley, D. A. Callahan, P. M. Celliers, C. J. Cerjan, D. S. Clark, E. L. Dewald, S. N. Dixit, T. Döppner, D. H. Edgell, R. Epstein, S. Glenn, G. Grim, S. W. Haan, B. A. Hammel, D. Hicks, W. W. Hsing, O. S. Jones, S. F. Khan, J. D. Kilkenny, J. L. Kline, G. A. Kyrala, O. L. Landen, S. Le Pape, B. J. MacGowan, A. J. Mackinnon, A. G. MacPhee, N. B. Meezan, J. D. Moody, A. Pak, T. Parham, H.-S. Park, J. E. Ralph, S. P. Regan, B. A. Remington, H. F. Robey, J. S. Ross, B. K. Spears, V. Smalyuk, L. J. Suter, R. Tommasini, R. P. Town, S. V. Weber, J. D. Lindl, M. J. Edwards, S. H. Glenzer, and E. I. Moses, Phys. Rev. Lett. **111**, 085004 (2013).
[38]S. P. Regan, R. Epstein, B. A. Hammel, L. J. Suter, H. A. Scott, M. A. Barrios, D. K. Bradley, D. A. Callahan, C. Cerjan, G. W. Collins, S. N. Dixit, T. Döppner, M. J. Edwards, D. R. Farley, K. B. Fournier, S. Glenn, S. H. Glenzer, I. E. Golovkin, S. W. Haan, A. Hamza, D. G. Hicks, N. Izumi, O. S. Jones, J. D. Kilkenny, J. L. Kline, G. A. Kyrala, O. L. Landen, T. Ma, J. J. MacFarlane, A. J. MacKinnon, R. C. Mancini, R. L. McCrory, N. B. Meezan, D. D. Meyerhofer, A. Nikroo, H.-S. Park, J. Ralph, B. A. Remington, T. C. Sangster, V. A. Smalyuk, P. T. Springer, and R. P. J. Town, Phys. Rev. Lett. **111**, 045001 (2013).
[39]R. Betti, P. Y. Chang, B. K. Spears, K. S. Anderson, J. Edwards, M. Fatenejad, J. D. Lindl, R. L. McCrory, R. Nora, and D. Shvarts, Phys. Plasmas **17**, 058102 (2010).
[40]B. K. Spears, private communication (2014); B. K. Spears, S. Glenzer, M. J. Edwards, S. Brandon, D. Clark, R. Town, C. Cerjan, R. Dylla-Spears, E. Mapoles, D. Munro, J. Salmonson, S. Sepke, S. Weber, S. Hatchett, S. Haan, P. Springer, E. Moses, J. Kline, G. Kyrala, and D. Wilson, Phys. Plasmas **19**, 056316 (2012).
[41]P. Patel, P. Springer, C. Cerjan, T. Ma, N. Izumi, D. Clark, B. Spears, M. Key, N. Landen, J. Lindl, and J. Edwards, in *Bulletin of the 55th Annual Meeting of the American Physical Society Division of Plasma Physics* (2012), Paper No. NO4.00001.
[42]C. Cerjan, P. T. Springer, and S. M. Sepke, Phys. Plasmas **20**, 056319 (2013).
[43]H.-S. Bosch and G. M. Hale, Nucl. Fusion **32**, 611-31 (1992).
[44]S. Atzeni and J. Meyer-ter-Vehn, *The Physics of Inertial Fusion* (Oxford University Press, 2004), p. 32.
[45]O. N. Krokhin and V. B. Rozanov, Sov. J. Quantum Electron. **2**, 393–394 (1973).
[46]S. E. Bodner, D. G. Colombant, A. J. Schmitt, and M. Klapisch, Phys. Plasmas **7**, 2298 (2000).
[47]V. N. Goncharov, J. P. Knauer, P. W. McKenty, P. B. Radha, T. C. Sangster, S. Skupsky, R. Betti, R. L. McCrory, and D. D. Meyerhofer, Phys. Plasmas **10**, 1906 (2003).
[48]S. A. MacLaren, M. B. Schneider, K. Widmann, J. H. Hammer, B. E. Yoxall, J. D. Moody, P. M. Bell, L. R. Benedetti, D. K. Bradley, M. J. Edwards, T. M. Guymer, D. E. Hinkel, W. W. Hsing, M. L. Kervin, N. B. Meezan, A. S. Moore, and J. E. Ralph, Phys. Rev. Lett. (in press).
[49]E. L. Dewald, J. Milovich, C. Thomas, J. Kline, C. Source, S. Glenn, and O. L. Landen, Phys. Plasmas **18**, 092703 (2011).
[50]E. L. Dewald, J. L. Milovich, P. Michel, O. L. Landen, J. L. Kline, S. Glenn, O. Jones, D. H. Kalantar, A. Pak, H. F. Robey, G. A. Kryala, L. Divol, L. R. Benedetti, J. Holder, K. Widmann, A. Moore, M. B. Schneider, T. Döppner, R. Tommasini, D. K. Bradley, P. Bell, B. Ehrlich, C. A. Thomas, M. Shaw, C. Widmayer, D. A. Callahan, N. B. Meezan, R. P. J. Town, A. Hamza, B. Dzenitis, A. Nikroo, K. Moreno, B. Van Wonterghem, A. J. Mackinnon, S. H. Glenzer, B. J. MacGowan, J. D. Kilkenny, M. J. Edwards, L. J. Atherton, and E. I. Moses, Phys. Rev. Lett. **111**, 235001 (2013).
[51]E. L. Dewald, L. J. Suter, C. Thomas, S. Hunter, D. Meeker, N. Meezan, S. H. Glenzer, E. Bond, J. Kline, S. Dixit, R. L. Kauffman, J. Kilkenny, and O. L. Landen, J. Phys.: Conf. Ser. **244**, 022074 (2010).
[52]E. L. Dewald, C. Thomas, S. Hunter, L. Divol, N. Meezan, S. H. Glenzer, S. J. Suter, E. Bond, J. L. Kline, J. Celeste, D. Bradley, P. Bell, R. L. Kauffman, J. Kilkenny, and O. L. Landen, Rev. Sci. Instrum. **81**, 10D938 (2010).
[53]D. G. Hicks, N. B. Meezan, E. L. Dewald, A. J. Mackinnon, R. E. Olson, D. A. Callahan, T. Döppner, L. R. Benedetti, D. K. Bradley, P. M. Celliers, D. S. Clark, P. Di Nicola, S. N. Dixit, E. G. Dzenitis, J. E. Eggert, D. R. Farley, J. A. Frenje, S. M. Glenn, S. H. Glenzer, A. V. Hamza, R. F. Heeter, J. P. Holder, N. Izumi, D. H. Kalantar, S. F. Khan, J. L. Kline, J. J. Kroll, G. A. Kyrala, T. Ma, A. G. MacPhee, J. M. McNaney, J. D. Moody, M. J. Moran, B. R. Nathan, A. Nikroo, Y. P. Opachich, R. D. Petrasso, R. R. Prasad, J. E. Ralph, H. F. Robey, H. G. Rinderknecht, J. R. Rygg, J. D. Salmonson, M. B. Schneider, N. Simanovskaia, B. K. Spears, R. Tommasini, K. Widmann, A. B. Zylstra, G. W. Collins, O. L. Landen, J. D. Kilkenny, W. W. Hsing, B. J. MacGowan, L. J. Atherton, and M. J. Edwards, Phys. Plasmas **19**, 122702 (2012).